

Mix and match networks: cross-modal alignment for zero-pair image-to-image translation

Yaxing Wang · Luis Herranz · Joost van de Weijer

Received: date / Accepted: date

Abstract This paper addresses the problem of inferring unseen cross-modal image-to-image translations between multiple modalities. We assume that only some of the pairwise translations have been seen (i.e. trained) and infer the remaining unseen translations (where training pairs are not available). We propose mix and match networks, an approach where multiple encoders and decoders are aligned in such a way that the desired translation can be obtained by simply cascading the source encoder and the target decoder, even when they have not interacted during the training stage (i.e. unseen). The main challenge lies in the alignment of the latent representations at the bottlenecks of encoder-decoder pairs. We propose an architecture with several tools to encourage alignment, including autoencoders and robust side information and latent consistency losses. We show the benefits of our approach in terms of effectiveness and scalability compared with other pairwise image-to-image translation approaches. We also propose zero-pair cross-modal image translation, a challenging setting where the objective is inferring semantic segmentation from depth (and vice-versa) without explicit segmentation-depth pairs, and only from two (disjoint) segmentation-RGB and depth-RGB training sets. We observe that a certain part of the shared information between unseen modalities might not be reachable, so we further propose a variant that leverages pseudo-pairs which allows us to exploit this shared information between the unseen modalities.

1 Introduction

For many computer vision applications, the task is to estimate a mapping between an input image and an output image. This family of methods is often known as image-to-image translations (image translations hereinafter). They include transformations between different modalities, such as from RGB to depth (Liu et al., 2016), or domains, such as luminance to color images (Zhang et al., 2016), or editing operations such as artistic style changes (Gatys et al., 2016). These mappings can also include other 2D representations such as semantic segmentations (Long et al., 2015) or surface normals (Eigen and Fergus, 2015). One drawback of the initial research on image translations is that the methods required paired data to train the mapping between the domains (Long et al., 2015; Eigen and Fergus, 2015; Isola et al., 2017). Another class of algorithms, based on cycle consistency, address the problem of mapping between unpaired domains (Kim et al., 2017; Yi et al., 2017; Zhu et al., 2017a). These methods are based on the observation that translating from one domain to another and translating back to the original domain should result in recovering the original input image.

The discussed approaches consider translations between two domains which are either paired or unpaired. However, for many real-world applications there exist both paired and unpaired domains simultaneously. Consider the case of image translation between multiple modalities, where for some of them we have access to aligned data pairs but not for all modalities. The aim would then be to exploit the knowledge from the paired modalities to obtain an improved mapping for the unpaired modalities. An example of such a translation setting is the following: you have access to a set of RGB images and their semantic segmentation, and a (differ-

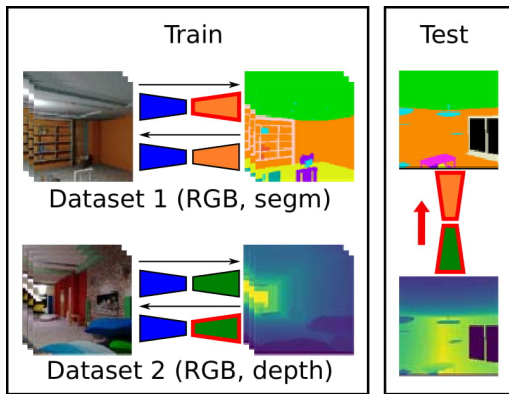


Fig. 1: Overview of mix and match networks (M&MNet) and zero-pair translation. Two disjoint datasets are used to train seen translations between RGB and segmentation and between RGB and depth (and vice versa). We want to infer the unseen depth-to-segmentation translation (i.e. *Zero-pair translation*). The M&MNet approach builds the unseen translator by simply cascading the source encoder and target decoder (i.e. depth and segmentation, respectively). Best viewed in color.

ent) set of RGB images and their corresponding depth maps, but you are interested in obtaining a mapping from depth to semantic segmentation (see Figure 1). We call this the *unseen* translation because we do not have pairs for this translation, and we refer to this setting as *zero-pair translation*. Zero-pair translation is typically desired when we extend an experimental setup with an additional camera in another modality. We now would like to immediately exploit this new sensor without the cost of labelling new data. In this paper, we provide a new approach to address the zero-pair translation problem.

We propose a new method, which we call *mix and match networks*, which addresses the problem of learning a mapping between unpaired modalities by seeking alignment between encoders and decoders via their latent spaces¹. The translation between unseen modalities is performed by simply concatenating the source modality encoder and the target modality decoder (see Figure 1). The success of the method depends on the alignment of the encoder and decoder for the unseen translation. We study several techniques that contribute to achieve alignment, including the usage of autoencoders, latent space consistency losses and the usage of robust side information to guide the reconstruction of spatial structure.

¹ The code is available online at <http://github.com/yaxingwang/Mix-and-match-networks>.

We evaluate our approach in a challenging cross-modal task, where we perform zero-pair depth to semantic segmentation translation (or semantic segmentation to depth translation), using only RGB-depth and RGB-semantic segmentation pairs during training. Furthermore, we show that the results can be further improved by using pseudo-pairs between the unseen modalities that allow the network to exploit unseen shared information. We also show that our approach can be used for cross-modal translation and with unpaired data. In particular, we show that mix and match networks scale better with the number of modalities, since they are not required to learn all pairwise image translation networks (i.e. they scale linearly instead of quadratically).

This article is an extended version of a previous conference publication (Wang et al., 2018b). We have included more analysis and insight about how mix and match networks exploit the information shared between modalities, and propose an improved mix and match networks framework with pseudo-pairs which allows us to access previously unexploited shared information between unseen modalities (see Section 5). This was found to significantly improve performance. In addition, Wang et al. (2018b) only report results on a synthetic dataset. Here we also provide results on real images (SUN RGB-D dataset (Song et al., 2015)) and four modalities (Freiburg Forest dataset (Valada et al., 2016)). Furthermore, we have added more insights on how the alignments between encoders and decoders evolve during training.

2 Related work

In this section we discuss the literature of related research areas.

2.1 Image-to-image translation

Paired translations Generic encoder-decoder architectures have achieved impressive results in a wide range of transformations between images. Isola et al. (2017) proposed *pix2pix*, which is a conditional generative adversarial network (conditional GAN) (Goodfellow et al., 2014; Mirza and Osindero, 2014) trained with pairs of input and output images to learn a variety of image translations. Those translations include cross-domain image translations such as colorization and style transfer. Gonzalez-Garcia et al. (2018) disentangle the information of the domains in the latent space, which allows to do cross-domain retrieval as well as perform one-to-many translations. The ability of

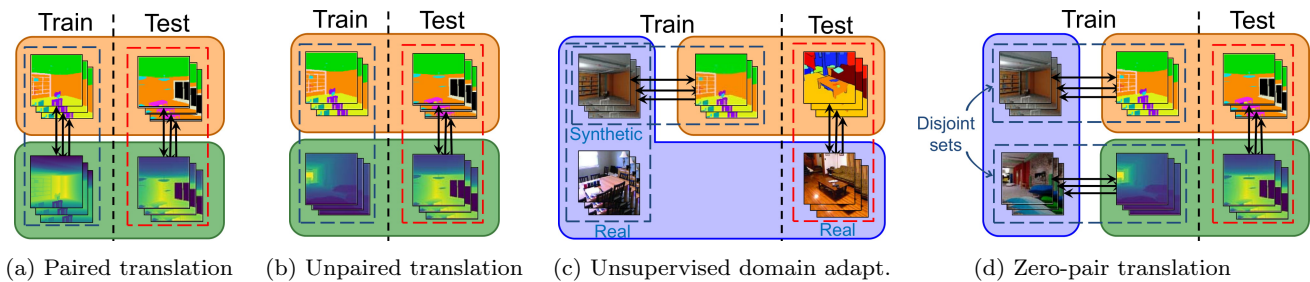


Fig. 2: cross-modal translation train and test settings: (a) paired translation, (b) unpaired translation, (c) unsupervised domain adaptation for segmentation (two modalities and two domains in the RGB modality), (d) zero-paired translation (three modalities). Best viewed in color.

GANs to generate realistic images also enables *pix2pix* to address effectively challenging cross-modal translations, such as semantic segmentation to RGB image. In this case, recent multi-scale architectures (Chen and Koltun, 2017; Wang et al., 2018a) achieve better results in higher resolution images.

Unpaired translations Various works extended image translation to the case where no explicit input-output image pairs are available (*unpaired* image translation), using the idea of cyclic consistency (Kim et al., 2017; Yi et al., 2017; Zhu et al., 2017a; Lin et al., 2018) or consistency between certain extracted features (Taigman et al., 2017). To avoid accidental artifacts and improve learning, Mejjati et al. (2018) integrate an attention mechanism to help translations focus on semantically meaningful regions. Liu et al. (2017) show that unsupervised mappings can be learned by imposing a joint latent space between the encoder and the decoder. Both TransGaGa (Wu et al., 2019) and TraV-eLGAN (Amodio and Krishnaswamy, 2019) address the issues of image translation across large geometry variations. The former disentangles image space in a Cartesian product of the appearance and the geometry latent spaces, and the latter considers a Siamese network to replace the cycle-consistency constraint.

In this work, we consider the case where paired data is available between some modalities and not available between others (i.e. zero-pair), and how the knowledge can be transferred to those unseen translations. Whereas previous work has focused on unpaired domains of the same modality, we show results for unpaired domains of different modalities.

Diversity in translations Given an input image (e.g. an edge image or a grayscale image) there are often multiple possible solutions (e.g. different plausible colorizations). The paired translation framework was extended to one-to-many translations in the work of Zhu et al. (2017b). DRIT (Lee et al., 2018), MUNIT (Huang et al., 2018) and Augmented CycleGAN (Almahairi et al.,

2018) can learn one-to-many translations in unpaired settings. In general, disentangled representations allow achieving diversity by keeping the content component and sampling the style component of the latent representation (Mathieu et al., 2016; Gonzalez-Garcia et al., 2018; Lee et al., 2018). Cho et al. (2019) propose a novel group-wise deep whitening-and-coloring method to improve computational efficiency. Alharbi et al. (2019) scale the latent filter to avoid a complicated network framework to perform one-to-many translations.

Multi-domain translations We also consider the case of multiple domains (and modalities). In concurrent work, Choi et al. (2018) also address scaling to multiple domains by using a single encoder-decoder model, which was previously explored by Perarnau et al. (2016). Chen et al. (2019) effectively disentangle the intermediate states between source and target domains. Wang et al. (2019) perform diverse and scalable image transfer by a single model. These works focus on faces and changing relatively superficial and localized attributes such as make-up, hair color, gender, etc., always within the RGB modality. In contrast, our approach uses multiple cross-aligned modality-specific encoders and decoders, which are necessary to address the deeper structural changes required by our cross-modal setting. Anosheh et al. (2018) also use multiple encoders-decoders but focus on the easier cross-domain task of style transfer.

2.2 Semantic segmentation and depth estimation

Semantic image segmentation aims at assigning each pixel to an object class. Long et al. (2015) propose fully convolutional networks (FCN), following an encoder-decoder structure. Since the FCN shows outstanding performance, this paradigm has been adopted in many current methods for semantic segmentation (Badrinarayanan et al., 2015; Ronneberger et al., 2015; Yu and Koltun, 2016; Chen et al., 2018; Zhao et al., 2017).

Of particular interest is SegNet (Badrinarayanan et al., 2015), which we adapt in our method. SegNet introduces the use of pooling indices instead of copying encoder features (i.e. skip connections, as in U-Net (Ronneberger et al., 2015)). We also consider pooling indices in our architecture for zero-pair image translation because we found them to be more robust and invariant under unseen translations.

Depth estimation aims at estimating the depth structure of an RGB image, usually represented as a depth map encoding the distance of each pixel to the camera. Most depth estimation methods are formalized as regression problems, where the aim is to minimize the mean squared error (MSE) with respect to a ground truth depth map. In general, an encoder-decoder architecture is used, often incorporating multiscale networks and skip connections (Liu et al., 2016; Wang et al., 2015; Roy and Todorovic, 2016; Eigen and Fergus, 2015; Kim et al., 2016; Kuznetsov et al., 2017; Laina et al., 2016).

Multi-modal encoder-decoders With the development of multi-sensor cameras and datasets (Lai et al., 2011; Silberman et al., 2012; Song et al., 2015), encoder-decoder architectures have been adapted to multi-modal inputs (Ngiam et al., 2011), where different modalities (e.g. RGB, depth, infrared, surface normals) are encoded and combined prior to the decoding. The network is trained to perform tasks such as multi-modal object recognition (Eitel et al., 2015; Cheng et al., 2016; Song et al., 2015), scene recognition (Song et al., 2017, 2015), object detection (Gupta et al., 2016) (with simple classifiers or regressors as decoders in these cases) and semantic segmentation (Silberman et al., 2012; Kendall et al., 2018; Wang and Neumann, 2018). Similarly, multi-task learning can be applied to reconstruct multiple modalities (Eigen and Fergus, 2015; Kendall et al., 2018). For instance Eigen and Fergus (2015) estimate depth, surface normals and semantic segmentation from a single RGB image, which can be seen as cross-modal translation.

Training a multi-task multimodal encoder-decoder network was recently studied by Kuga et al. (2017). They use a joint latent representation space for the various modalities. In our work we consider the alignment and transferability of pairwise image translations to unseen translations, rather than joint encoder-decoder architectures. Another multimodal encoder-decoder network was studied by Cadena et al. (2016). They show that multi-modal autoencoders can address the depth estimation and semantic segmentation tasks simultaneously, even in the absence of some of the input modalities. All these works do not consider the zero-pair image translation problem addressed in this paper.

2.3 Zero-shot recognition

In conventional supervised image recognition, the objective is to predict the class label that is provided during training. However, this poses limitations in scalability to new classes, since new training data and annotations are required. In zero-shot learning (Lampert et al., 2014; Fu et al., 2017; Xian et al., 2018a,b; Akata et al., 2016), the objective is to predict an unknown class for which there is no image available, but a description of the class (i.e. *class prototype*) or any other source of semantic similarity with seen classes. This description can be a set of attributes (e.g. has wings, blue, four legs, indoor) (Lampert et al., 2014; Jayaraman and Grauman, 2014), concept ontologies (Fergus et al., 2010; Rohrbach et al., 2011) or textual descriptions (Reed et al., 2016). In general, an intermediate semantic space is leveraged as a bridge between the visual features from seen classes and class description from unseen ones. In contrast to zero-shot recognition, we focus on unseen translations (unseen input-output pairs rather than simply unseen class labels).

2.4 Zero-pair language translation

Evaluating models on unseen language pairs has been studied recently in machine translation (Johnson et al., 2016; Chen et al., 2017; Zheng et al., 2017; Firat et al., 2016). Johnson et al. (2016) proposed a neural language model that can translate between multiple languages, even pairs of language where no explicit paired sentences were provided². In their method, the encoder, decoder and attention are shared. In our method we focus on images, which are essentially a radically different type of data, with two dimensional structure in contrast to the sequential structure of language.

2.5 Domain adaptation

A related line of research is unsupervised domain adaptation. In that case the task is to transfer knowledge from a supervised source domain to an unsupervised target domain (see Figure 2c). This problem has been addressed by finding domain invariant feature spaces (Gong et al., 2012; Ganin and Lempitsky, 2015; Tsai et al., 2018), using image translation models to map between source and target domain (Wu

² Note that Johnson et al. (2016) refers to this as *zero-shot* translation. In this paper we refer to this setting as *zero-pair* to emphasize that what is unseen is paired data and avoid ambiguities with traditional zero-shot recognition which typically refers to unseen samples.

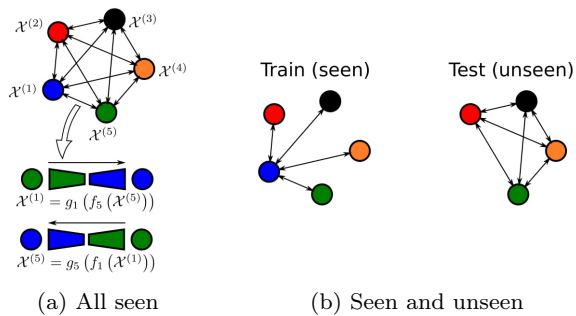


Fig. 3: Multi-domain image translation using pairwise translations: (a) all translations are seen during training, and (b) our setting: some translations are seen, then test on unseen. Best viewed in color.

et al., 2018), and exploiting pseudo-labels (Saito et al., 2017; Zou et al., 2018). Knowledge can also be transferred across modalities (Gupta et al., 2016; Castrejon et al., 2016; Hoffman et al., 2016b,a). For instance, Gupta et al. (2016) use cross-modal distillation to learn depth models for classification by distilling RGB features (from pretrained model trained on a much larger RGB dataset), through a large set of unlabeled RGB-D pairs. Modality adaptation can also be achieved using cross-modal translation (Xu et al., 2017; Zhang et al., 2019).

When comparing this line of research with the setting we consider in this paper (i.e. zero-pair translation) there are some important differences. The unsupervised domain adaptation setting (see Figure 2c) typically involves two modalities (e.g. RGB and segmentation), and two domains within the RGB modality (e.g. synthetic and real). Paired data is available only for the synthetic-segmentation while the synthetic-real translation is unpaired, and the unseen translation is real-segmentation (with test paired data). In contrast, our setting (see Figure 2d) is more challenging involving three modalities, with one disjoint paired training set for each seen translation. In comparison, using paired data to tackle domain shift allows us to reach much larger and challenging domain shifts and even modality shifts, a setting which, to the best of our knowledge, is not considered in the domain adaptation literature.

3 Multi-modal image translations

We consider the problem of image translation between multiple modalities. In particular, a translation from a source modality $\mathcal{X}^{(i)}$ to a target modality $\mathcal{X}^{(j)}$ is a mapping $T_{ij}: x^{(i)} \mapsto x^{(j)}$. This mapping is implemented as an encoder-decoder chain $x^{(j)} = T_{ij}(x^{(i)}) = g_j(f_i(x^{(i)}))$ with source encoder f_i and target decoder

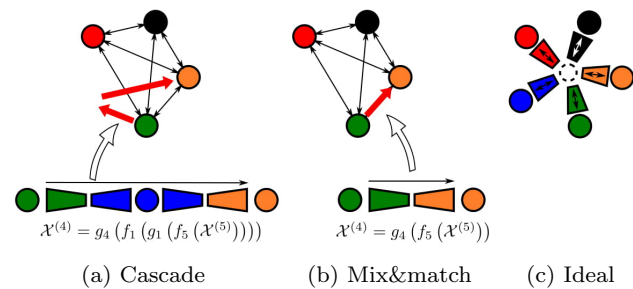


Fig. 4: Inferring unseen translations: (a) cascading translators, (b) mix and match networks (M&MNs), and (c) ideal case of encoders-decoders with aligned representations. Best viewed in color.

g_j . Translations between modalities connected during training are all learned jointly, and in both directions. Note that the encoder and decoder of translation T_{ij} are different from those of T_{ji} . In order to perform any arbitrary translation between modalities, all pairwise translations must be trained (i.e. seen) during the training stage (see Figure 3a).

In this article we address the case where only a subset of the translations are seen during training, while the rest remain unseen (see Figure 3b). Our objective is to be able to infer these unseen translations during test time.

3.1 Inferring unseen translations

In the case where some of the translations are unseen during training, we could still try to infer them by reusing the available networks. Here we discuss two possible ways: *cascading translators*, which we use as baseline, and the proposed *mix and match networks* approach.

Cascaded translators Assuming there is a path of seen translations between the source modality and the target modality via intermediate modalities (see Figure 3b), a possible solution is simply concatenating the seen translators across this path. This will result in a mapping from the source to the target modality by reconstructing images in the intermediate modalities (see Figure 4a). However, the success of this approach depends on the effectiveness of the intermediate translators.

Unpaired translators An alternative is to frame the problem as unpaired translation between the source and target modalities and disregard the other modalities, learning a translation using methods based on cycle consistency (Zhu et al., 2017a; Kim et al., 2017; Yi et al., 2017; Liu et al., 2017). This approach requires

training an unpaired translator per unseen translation. In general, unpaired translation can be effective when the translation is within the same modality and involves a relatively small shift between source and target domains (e.g. body texture in horse-to-zebra), but struggles in the more challenging case of cross-modal translations.

Mix and match networks (M&MNNets) We propose to obtain the unseen translator by simply concatenating the encoder of the source modality and the decoder of the target modality (see Figure 4b). The problem is that these two networks have not directly interacted during training, and therefore, for this approach to be successful, the two latent spaces must be aligned.

3.2 Aligning for unseen translations

The key challenge in M&MNNets is to ensure that the latent representation from the encoders can be decoded by all decoders, including those unseen (see Figure 4c). In order to address this challenge, encoders and decoders must be aligned in their latent representations. In addition, the encoder-decoder pair should be able to preserve the spatial structure, even in unseen translations.

In the following we describe the different techniques we use to enforce feature alignment between unseen encoder-decoder pairs.

Shared encoders and decoders Sharing encoders and decoders is a basic requirement to reuse latent representations and reduce the number of networks.

Autoencoders We jointly train modality-specific autoencoders with the image translation networks. By sharing the weights between the auto-encoders and the image translation encoder-decoder pairs the latent space is forced to align.

Robust side information In general, image translation tasks result in output images with similar spatial structure as the input ones, such as scene layouts, shapes and contours that are preserved across the translation. In fact, this spatial structure available in the input image is critical to simplify the problem and achieve good results, especially in cross-modal translations. Successful image translation methods often use multi-scale intermediate representations from the encoder as side information to guide the decoder in the upsampling process. Examples of side information are skip connections (He et al., 2016; Ronneberger et al., 2015) and pooling indices (Badrinarayanan et al., 2015; Li et al., 2018). We exploit side information in cross-modal translation (see discussion in Section 4.4).

Latent space consistency (only in paired settings) When paired data between some modalities is available, we can enforce consistency in the latent representations of each direction of the translations. Taigman et al. (2017) use L2 distance between a latent representation and the reconstructed after another decoding and encoding cycle. Here we enforce the representations $f_i(x^{(i)})$ and $f_j(x^{(j)})$ of two paired samples $(x^{(i)}, x^{(j)})$, to be aligned, since both images represent the same content (just in two different modalities). This is done by introducing a latent space consistency loss which is defined as $\|f_i(x^{(i)}) - f_j(x^{(j)})\|_2$. We exploit this constraint in zero-pair image translation (see Section 4).

Adding noise to latent space The latent space consistency we apply is based on reducing the difference between the $f_i(x^{(i)})$ and $f_j(x^{(j)})$. The network can minimize this loss by aligning the representations of $f_i(x^{(i)})$ and $f_j(x^{(j)})$, but it could also minimize it by just reducing the signal $\|f_i(x^{(i)})\|$ and $\|f_j(x^{(j)})\|$. This would reduce the latent space consistency loss but not improve the alignment. Adding noise to the output of each encoder prevents this problem, since reducing the signal would then hurt the translation and auto-encoder losses. In practice, we found that adding noise helps to train the networks and improves the results during test.

3.3 Scalable image translation with M&MNNets

As the number of modalities increases, the number of pairwise translations grows quadratically. Training encoder-decoder pairs for all pairwise translations in N modalities would require $N \times (N - 1)/2$ encoders and $N \times (N - 1)/2$ decoders (see Figure 3a). One of the advantages of M&MNNets is their better *scalability*, since many of those translations can be inferred without explicitly training them (see Figure 3b). It requires that each encoder and decoder should be involved in at least one translation pair during training in order to be aligned with the others, thereby reducing complexity from quadratic to linear with the number of modalities (i.e. N encoders and N decoders).

3.4 Translating domains instead of modalities

Although we described the proposed framework for cross-modal translation, the same framework can be easily adapted to cross-domain image translation. In that case, the modality is the same (typically RGB) and the translation is arguably less complex since the

network does not need to learn to change the modality, just the domain. It can be learned sometimes with unpaired data (e.g. style transfer, face attributes and expressions).

Here we use cross-domain image translation to illustrate the scalability of M&MNet. The datasets (color and artworks) and the network architectures are provided in Appendix B. Figure 5 shows two examples involving multi-domain unpaired image translation. Figure 5a-b shows an image recoloring application with eleven domains ($N = 11$). Images are objects in the colored objects dataset (Yu et al., 2018), where we use colors as domains. A naive solution is training all pairwise recoloring combinations with CycleGANs, which requires training a total of $N(N-1)/2 = 55$ encoders (and decoders). In contrast, M&MNet only require to train eleven encoders and eleven decoders, while still successfully addressing the recoloring task. In particular, all translations from or to the blue domain are trained, while the remaining translations not involving blue are unseen. The input images (framed in red) and the resulting seen translations (framed in blue) are shown in Figure 5a. The additional images in Figure 5b correspond to the remaining unseen translations.

We also illustrate M&MNet in a style transfer setting with five domains. They include photo (used as anchor domain) and four artistic styles with data from Zhu et al. (2017a). M&MNet can reasonably infer unseen translations between styles (see Figure 5d) using only five encoders and five decoders (for a total of twenty possible translations). Note that the purpose of these examples is to illustrate the scalability aspect of M&MNet in multiple domains, not to compete with state-of-the-art recoloring or style transfer methods.

4 Zero-pair cross-modal translation

Well aligned M&MNet can be applied to a variety of problems. Here, we apply them to a challenging setting we call *zero-pair cross-modal translation*, which involves three modalities³. Note that cross-modal translations usually require modality-specific architectures and losses.

4.1 Problem definition

We consider the problem of jointly learning two seen cross-modal translations: RGB-to-segmentation translation $y = T_{RS}(x)$ (and $x = T_{SR}(y)$) and RGB-to-

depth translation $z = T_{RD}(x)$ (and $x = T_{DR}(z)$) and evaluating on the unseen depth-to-segmentation transformations $y = T_{DS}(z)$ and $z = T_{SD}(y)$ (see Figures 1 and 2c). In contrast to the conventional unpaired translation setting, here seen translations have paired data (cross-modal translation is difficult to learn without paired samples). In particular, we consider the case where the former translations are learned from a semantic segmentation dataset \mathcal{D}_{RS} with pairs $(x, y) \in \mathcal{D}_{RS}$ of RGB images and segmentation maps, and the second from a disjoint RGB-D dataset \mathcal{D}_{RD} with pairs of RGB and depth images $(x, z) \in \mathcal{D}_{RD}$. Therefore no pairs with matching depth images and segmentation maps are available to the system. The system is evaluated on a third dataset \mathcal{D}_{DS} with paired depth images and segmentation maps.

4.2 Mix and match networks architecture

The overview of the framework is shown in Figure 6. As basic building blocks we use three modality-specific encoders $f_R(x)$, $f_D(z)$ and $f_S(y)$ (RGB, depth and semantic segmentation, respectively), and the corresponding three modality-specific decoders $g_R(h)$, $g_D(h)$ and $g_S(h)$, where h is the latent representation in the shared space. The required translations are implemented as $y = T_{RS}(x) = g_S(f_R(x))$, $z = T_{RD}(x) = g_D(f_R(x))$ and $y = T_{DS}(z) = g_S(f_D(z))$.

Encoder and decoder weights are shared across the different translations involving same modalities (same color in Figure 6). To enforce better alignment between encoders and decoders of the same modality, we also include self-translations using the corresponding three autoencoders $T_{RR}(x) = g_R(f_R(x))$, $T_{DD}(y) = g_D(f_D(y))$ and $T_{SS}(z) = g_S(f_S(z))$.

We base our encoders and decoders on the SegNet architecture (Badrinarayanan et al., 2015). The encoder of SegNet itself is based on the 13 convolutional layers of the VGG-16 architecture (Simonyan and Zisserman, 2015). The decoder mirrors the encoder architecture with 13 deconvolutional layers. Weights in encoders and decoders are randomly initialized following a standard Gaussian distribution except for the RGB encoder which is pretrained on ImageNet (Deng et al., 2009).

As in SegNet, pooling indices at each downsampling layer of the encoder are provided to the corresponding upsampling layer of the (seen or unseen) decoder⁴. These pooling indices seem to be relatively sim-

³ For simplicity, we will refer to the output semantic segmentation maps and depth as modalities rather than tasks, as done in some works.

⁴ The RGB decoder does not use pooling indices, since in our experiments we observed undesired grid-like artifacts in the RGB output when we use them.

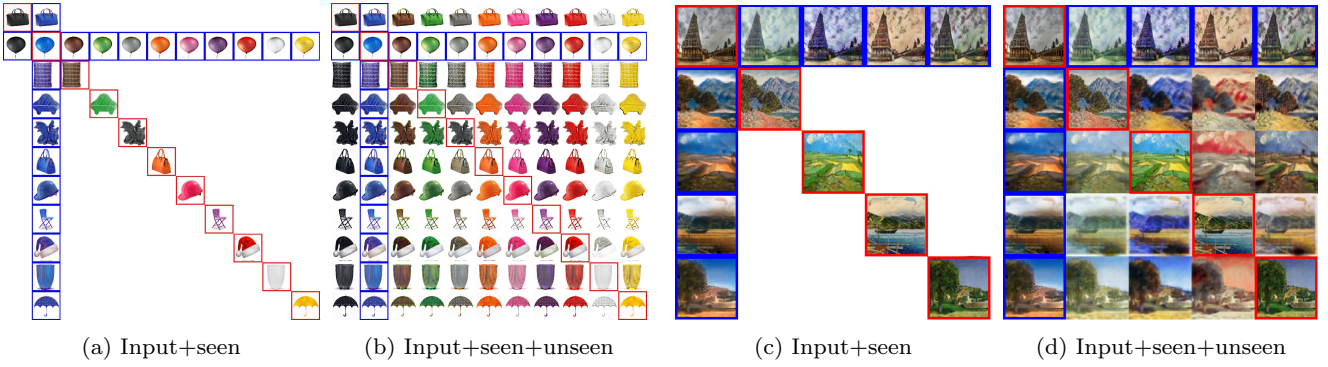


Fig. 5: Two examples of scalable inference of multi-domain translations with M&MNNets. Color transfer (a-b): only transformations from blue or to blue (anchor domain) are seen. Style transfer (c-d): trained on four styles + photo (anchor) with data from Zhu et al. (2017a). From left to right: photo, Monet, van Gogh, Ukiyo-e and Cezanne. Input images are highlighted in red and seen translations in blue. Best viewed in color.

ilar across the three modalities and effective to transfer spatial structure information that help to obtain better depth and segmentation boundaries in higher resolutions. Thus, they provide relatively modality-independent side information. We also experimented with skip connections and no side information at all.

4.3 Loss functions

As we mentioned before, for a correct cross-alignment between encoders and decoders, training is critical for zero-pair translation. The final loss combines a number of modality-specific losses for both cross-modal translation and self-translation (i.e. autoencoders) and alignment constraints in the latent space

$$L = \lambda_R L_{RGB} + \lambda_S L_{SEG} + \lambda_D L_{DEPTH} + \lambda_A L_{LAT}$$

where λ_R , λ_S , λ_D and λ_A are weights which balance the losses.

RGB We use a combination of pixelwise L2 distance and adversarial loss $L_{RGB} = \lambda_{L2} L_{L2} + L_{GAN}$. L2 distance is used to compare the ground truth RGB image and the output RGB image of the translation from a corresponding depth or segmentation image. It is also used in the RGB autoencoder

$$L_{L2} = \mathbb{E}_{(x,y) \sim \mathcal{D}_{RS}} [\|T_{SR}(y) - x\|_2] \quad (1)$$

$$+ \mathbb{E}_{(x,z) \sim \mathcal{D}_{RD}} [\|T_{DR}(z) - x\|_2] \quad (2)$$

$$+ \mathbb{E}_{x \sim \mathcal{D}_{RS} \cup \mathcal{D}_{RD}} [\|T_{RR}(x) - x\|_2] \quad (3)$$

In addition, we also include the least squares adversarial loss (Mao et al., 2016; Isola et al., 2017) on the output of the RGB decoder

$$L_{GAN} = \mathbb{E}_{x \sim \mathcal{D}_{RS} \cup \mathcal{D}_{RD}} [(C(x) - 1)^2] + \mathbb{E}_{\hat{x} \sim \hat{p}(x)} [(C(\hat{x}))^2]$$

where $\hat{p}(x)$ is the resulting distribution of the combined images \hat{x} generated by $\hat{x} = T_{SR}(y)$, $\hat{x} = T_{DR}(z)$ and $\hat{x} = T_{RR}(x)$. Note that the RGB autoencoder and the discriminator $C(x)$ are both trained with the combined RGB data \mathcal{X} .

Depth For depth we use the Berhu loss (Laina et al., 2016) in both RGB-to-depth translation and in the depth autoencoder

$$L_{DEPTH} = \mathbb{E}_{(x,z) \sim \mathcal{D}_{RD}} [\mathcal{B}(T_{RD}(x) - z)] \quad (4)$$

$$+ \mathbb{E}_{(x,z) \sim \mathcal{D}_{RD}} [\mathcal{B}(T_{DD}(z) - z)] \quad (5)$$

where $\mathcal{B}(z)$ is the average Berhu loss, which is given by

$$\mathcal{B}(z' - z) = \begin{cases} |z' - z| & |z' - z| \leq c \\ \frac{(z' - z)^2 + c^2}{2c} & |z' - z| > c \end{cases} \quad (6)$$

where $z' = T_{RD}(x)$, and $c = \frac{1}{5} \max_i (|z'_i - z_i|)$, where i indexes the pixels of each image.

Semantic segmentation For segmentation we use the average cross-entropy loss $\mathcal{CE}(\hat{y}, y)$ in both RGB-to-segmentation translation and the segmentation autoencoder

$$L_{SEM} = \mathbb{E}_{(x,y) \sim \mathcal{D}_{RS}} [\mathcal{CE}(T_{RS}(x), y)] \quad (7)$$

$$+ \mathbb{E}_{(x,y) \sim \mathcal{D}_{RS}} [\mathcal{CE}(T_{SS}(y), y)]. \quad (8)$$

Latent space consistency We enforce latent representations to remain close, independently of the encoder that generated them. In our case we have two latent space consistency losses

$$L_{LAT} = L_{LAT1} + L_{LAT2} \quad (9)$$

$$L_{LAT1} = \mathbb{E}_{(x,y) \sim \mathcal{D}_{RS}} [\|f_R(x) - f_S(y)\|_2] \quad (10)$$

$$L_{LAT2} = \mathbb{E}_{(x,z) \sim \mathcal{D}_{RD}} [\|f_R(x) - f_D(z)\|_2] \quad (11)$$

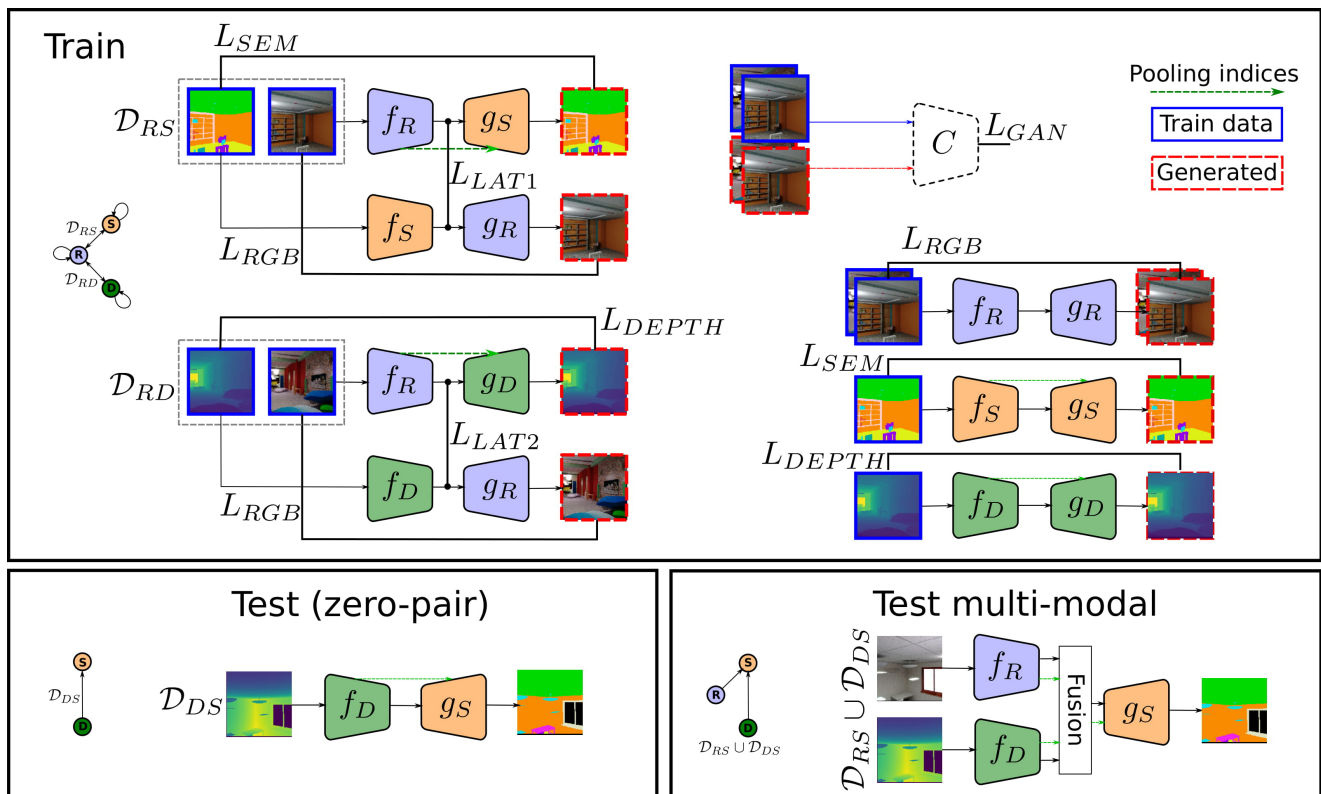


Fig. 6: Zero-pair cross-modal and multi-modal image translation with M&MNet. Two disjoint sets \mathcal{D}_{RS} and \mathcal{D}_{RD} are seen during training, containing (RGB,depth) pairs and (RGB,segmentation) pairs, respectively. The system is tested on the unseen translation depth-to-segmentation (zero-pair) and (RGB+depth)-to-segmentation (multimodal), using a third unseen set \mathcal{D}_{DS} . Encoders and decoders with the same color share weights. Note that we do not apply pooling indices for RGB decoders. Best viewed in color.

4.4 The role of side information

Spatial side information plays an important role in image translation, especially in cross-modal translation (e.g. semantic segmentation). Reconstructing images requires reconstructing spatial details. Side information from a particular encoder layer can provide helpful hints to the decoder about how to reconstruct the spatial structure at a specific scale and level of abstraction.

Skip connections Perhaps the most common type of side information connecting encoders and decoders comes in the form of *skip connections*, where the feature from a particular layer is copied and concatenated with another feature further in the processing chain. U-Net (Ronneberger et al., 2015) introduced a widely used architecture in image segmentation and image translation where convolutional layers in encoder and decoder are mirrored and the feature of a particular encoding layer is concatenated with the feature with the corresponding layer at the decoder. It is important to observe that skip connections make the decoder heavily condition on the particular features of the encoder. This

is not a problem in general because translations are usually seen during training and therefore latent representations are aligned. However, in our setting with unseen translations that conditioning is simply catastrophic, because the target decoder is only aware of the features in encoders from modalities seen during training. Otherwise, as in the case of an unseen encoder, the result is largely unpredictable.

Pooling indices The SegNet architecture (Badrinarayanan et al., 2015) includes unpooling layers that leverage pooling indices from the mirror layers of the encoder. Pooling indices capture the locations of the maximum values in the input feature map of a max pooling layer. These locations are then used to guide the corresponding unpooling operation in the decoder, helping to preserve finer details. Note that pooling indices are more compact descriptors than encoder features from skip connections, and since the unpooling operation is not learned, pooling indices are less dependent on the particular encoder and therefore more robust for unseen translations.

5 Shared information between unseen modalities

5.1 Shared and modality-specific information

The information conveyed by the latent representation is key to perform image translation. Encoders extract this information from the input image and decoders use it to reconstruct the output image. In general, this latent representation can contain information shared between the source and target modalities, and information specific to each modality. In a setting where the same latent representation is used across multiple encoders and decoders, the latent representation must capture information about all input and output modalities.

We can represent modalities as circles, whose intersections represent shared information between them. Figure 7a represents the particular case of zero-pair cross-modal translation with three modalities (described in the previous section). Note that translators and autoencoders force the latent representation to capture both shared and modality-specific information. However, the better the information shared between modalities is captured in the latent representation, the more effective cross-modal translations are.

The framework described in Section 4.2 enables the inference of unseen translations via the anchor modality RGB, whose encoder and decoder are shared across the two seen translations. That is the only component that indirectly enforces alignment of depth and segmentation encoders and decoders. Therefore, the latent information used in the unseen translation is the one shared by the three modalities.

In contrast, the information shared between depth and segmentation that is not shared with RGB (the dashed region in Figure 7a) is not exploited during training by depth and segmentation encoders and decoders, because it is of no use to solve any of the seen translations. This makes inferred translations less effective because depth and segmentation encoders are ignoring potentially useful information that could improve translation to segmentation and depth, respectively. In this section, we propose an extension of our basic framework that aims at explicitly enforcing alignment between unseen modalities in order to exploit all shared information between unseen modalities (see the highlighted region in Figure 7b). Since no training pairs between those modalities are available, that alignment requires to be between unpaired samples.

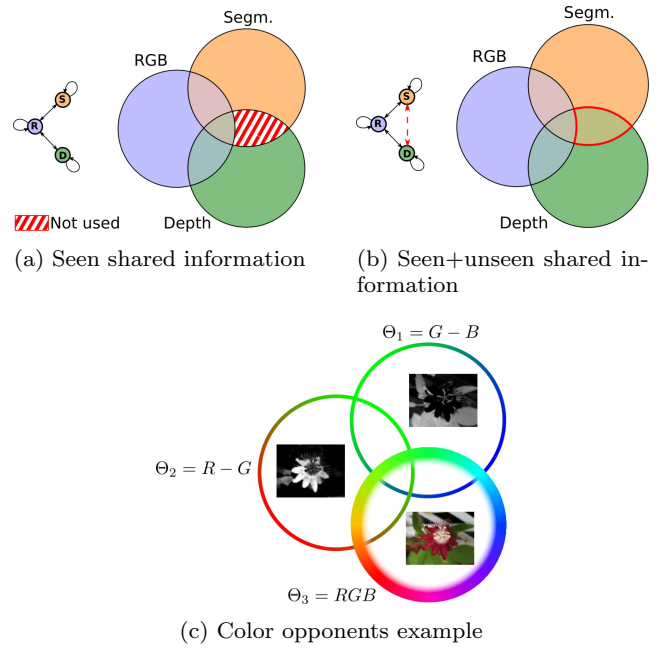


Fig. 7: Specific and shared information: (a) basic mix and match nets (see Fig 6) ignore depth-segmentation shared information, (b) extended mix and match net exploiting depth-segmentation shared information (unpaired information in our case), and (c) illustration using color opponents (trained on (Θ_1, Θ_2) and (Θ_1, Θ_3) , and evaluated on unseen translation (Θ_2, Θ_3)). Best viewed in color.

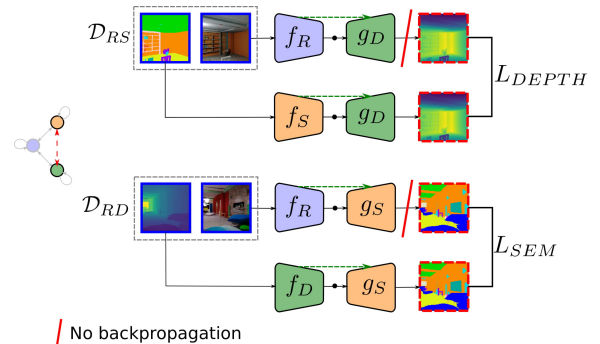


Fig. 8: Pseudo-pairs pipeline on the unseen translation. This pipeline is combined with the basic cross-modal M&MNs of Fig 6.

5.2 Exploiting shared information between unseen modalities

We adapt the idea of pseudo-labels, used previously in unsupervised domain adaptation (Saito et al., 2017; Zou et al., 2018), to our zero-pair cross-modal setting. The main idea is that we would also like to train directly the encoder-decoder between the unseen modal-

ities. However, since we have no paired data between these modalities, we propose to use pseudo-pairs.

In our specific zero-pair cross-modal setting, recall we use x , y , and z to respectively indicate data from the the RGB, semantic segmentation and depth modality. We use the encoder-decoder networks between the seen modalities to form the pseudo-pairs $(T_{RD}(x), y)$ and $(T_{RS}(x), z)$. Now we can also train encoders and decoders between the unseen modalities depth and segmentation (see Figure 8) using the following loss:

$$L_{PP} = \mathbb{E}_{(x,y) \sim \mathcal{D}_{RS}} [\mathcal{B}(T_{RD}(x) - T_{SD}(y))] \quad (12)$$

$$+ \mathbb{E}_{(x,z) \sim \mathcal{D}_{RD}} [\mathcal{CE}(T_{RS}(x), T_{DS}(z))] \quad (13)$$

where \mathcal{B} is the average Berhu loss (Laina et al., 2016), and \mathcal{CE} is the cross-entropy loss. The direct training of the encoder-decoder between the unseen modality allows us to exploit correlation between features in these modalities for which no evidence exists in the RGB modality (dashed region in Figure 7a). In practice we first train the network without the pseudo-labels. After convergence we add L_{PP} and train further with all losses until final convergence.

Note that this additional term encourages the segmentation-to-depth and depth-to-segmentation translators to exploit this shared information between the unseen modalities, including the previously ignored one, in order to improve the translation to match the one obtained from RGB. The latter is more accurate since it has been trained with paired samples. A problem with this approach is that this new loss can harm the training of seen translations from RGB, since pseudo-labels are less reliable than true labels. For this reason we do not update the weights of the translators involving RGB with the pseudo-pairs (this is indicated with the red line in Figure 8).

5.3 Pseudo-pair example

To illustrate the potential of pseudo-pairs we consider a cross-domain image translation example where the not-used part between the unpaired domains (striped region in Figure 7) is expected to be substantial. We consider the task of estimating an RGB image from a single channel. In particular, we consider the following three domains⁵

$$\begin{aligned} \Theta_1 &= R - G \\ \Theta_2 &= G - B \\ \Theta_3 &= (R, G, B) \end{aligned} \quad (14)$$

⁵ We choose the opponent channels because they are less correlated than the R, G and B channels (Geusebroek et al., 2001).

Type	Method	Accuracy (%)
Paired		
Seen	M&MNet s $\Theta_1 \rightarrow \Theta_3$	75.0
Zero-pair		
Unseen	M&MNet s $\Theta_2 \rightarrow \Theta_3$	36.5
	M&MNet s +PP $\Theta_2 \rightarrow \Theta_3$	57.5
Multi-modal		
Seen/unseen	M&MNet s $(\Theta_1, \Theta_2) \rightarrow \Theta_3$	77.5
	M&MNet s + PP $(\Theta_1, \Theta_2) \rightarrow \Theta_3$	80.5

Table 1: Flower classification accuracy obtained on Θ_3 computed for various image translation models. The importance of pseudo-pairs can be clearly seen.

where Θ_1 and Θ_2 are scalar images and Θ_3 is a three channel RGB image (see Figure 7c). Both domains Θ_1 and Θ_2 contain relevant and complementary information on estimating the RGB image.

For this experiment we use the ten most frequent classes of the Flower dataset (Nilsback and Zisserman, 2008) which are *passionflower*, *petunia*, *rose*, *wallflower*, *watercress*, *waterlily*, *cyclamen*, *foxglove*, *frangipani*, *hibiscus*. For training we have pairs (Θ_1, Θ_2) and (Θ_1, Θ_3) of non-overlapping images. For test we use a separate test set. To evaluate the quality of the computed RGB images, we apply a flower classification algorithm on them and report the classification accuracy (See Appendix C).

The results are presented in Table 1. In the first two rows the result of M&MNet s with and without pseudo-pairs are compared. The usage of pseudo-pairs results in a huge absolute performance gain of 21%. This shows that, for domains which have considerable amounts of complementary information, pseudo-pairs can significantly improve performance. In the next two rows, we have also included the multi-modal results. In this case the pseudo-pairs double the performance gain with respect to the paired domain (last row) from $77.5 - 75 = 2.5\%$ to $80.5 - 75 = 5.5\%$.

The qualitative results are provided in Figure 9. The results show the effectiveness of the pseudo-pairs. The method without the pseudo-pairs can only exploit information which is shared between the three domains. The domain Θ_1 contains information about the red-green color axes, and the mix and match nets (without pseudo-pairs) approach does partially manage to reconstruct that part (see first row Figure 9). However, Θ_1 has no access to the blue-yellow information which is encoded in the Θ_2 . Adding the pseudo-pairs allows to exploit this information and the reconstructed RGB images are closer to the ground truth image (see second and third row Figure 9).

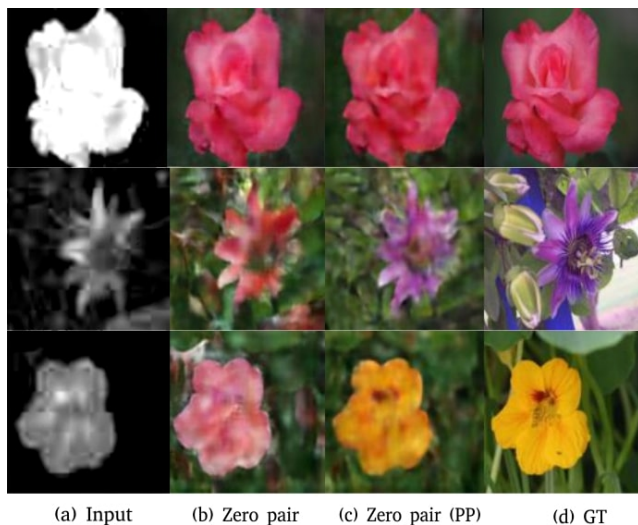


Fig. 9: Visualization of RGB image estimation in Flowers dataset. (a) input image from Θ_2 (via seen translation), (b) zero pair translation without pseudo-pairs (Wang et al., 2018b), (c) zero pair with the pseudo-pairs (PP), (d) ground truth.

6 Experiments

In this section we demonstrate the effectiveness of M&MNets and their variants to address unseen translations in the challenging cross-modal translation setting involving the modalities RGB, depth and segmentation.

6.1 Datasets and experimental settings

We use two RGB-D datasets annotated with segmentation maps, one with synthetic images and the other with real captured images. A third dataset also includes near infrared (NIR) as a fourth modality.

SceneNet RGB-D The SceneNet RGB-D dataset (McCormac et al., 2017) consists of 16865 synthesized training videos and 1000 test videos. Each of them contains 300 frames representing the same scene in a multi-modal triplet (RGB, depth and segmentation), with a size of 320x240 pixels. We collected 150K triplets for our training set, 10K triplets for our validation set and 10K triplets for our test set. The triplets are sampled uniformly from the first frame to the last frame every 30 frames. The triplets for the validation set are collected from the remaining training videos and the test set is taken from the test dataset.

In order to evaluate zero-pair translation, we divided the training set (and validation set) into two equal non-overlapping splits from different videos (to avoid covering the same scenes). We discard depth im-

ages in one set and segmentation maps in the other, thus creating two disjoint training sets with paired instances, \mathcal{D}_{RS} and \mathcal{D}_{RD} respectively, to train our model.

SUN RGB-D The SUN RGBD dataset (Song et al., 2015) contains 10335 real RGB-D images of room scenes. Each RGB image has a corresponding depth and segmentation map. We collected two sets: 10K triplets for the training set and 335 triplets for test set. For the training set, we split it into two disjoint subsets, one containing (RGB, segmentation) pairs, and the other containing (RGB, depth) pairs, each of them consisting of 5K pairs.

Freiburg Forest The Freiburg Forest dataset (Valada et al., 2016) consists of images of 1024x768. We crop images (RGB, depth, NIR and semantic segmentation) to 256x256. We consider five different semantic classes: *Sky*, *Trail*, *Grass*, *Vegetation* and *Obstacle*. Note we combine the *tree* and *vegetation* into a single class (*Vegetation*) as suggested in (Valada et al., 2016). We use the training and test datasets splits provided by the authors.

Network training We use Adam (Kingma and Ba, 2014) with a batch size of 6, using a learning rate of 0.0002. We set $\lambda_R = 1$, $\lambda_S = 100$, $\lambda_D = 10$, $\lambda_A = 1$, $\lambda_{L2} = 1$. We initially train the mix and match framework without autoencoders, without latent consistency losses, and without adding noise during the first 200K iterations. Then we freeze the RGB encoder, add the autoencoders, latent consistency losses and noise to the latent space, and for the following 200K iterations we use $\lambda_R = 10$, $\lambda_A = 10$, $\lambda_{L2} = 100$. We found that the network converges faster using a larger λ_A for the second stage. The noise is sampled from a Gaussian distribution with zero mean and a standard deviation of 0.5. For the variant with pseudo-pairs, in a third stage we include the pseudo-pair pipeline and the corresponding loss and train for another additional 100K iterations, using $\lambda_{PP} = 100$ and learning rate 0.00002. We experimentally found that the above setting also achieves outstanding performance on the Freiburg Forest dataset. The network information is displayed in Appendix A.

Evaluation metrics Following common practice, for the segmentation modality we compute the intersection over union (IoU) and per-class average (mIoU), and the global scores, which gives the percentage of correctly classified pixels. For the depth modality we also include quantitative evaluation, following the standard

error metrics for depth estimation (Eigen and Fergus, 2015):

$$\delta < = \frac{1}{|y|} \sum_{y_i \in y} [\delta(y_i, y'_i) < \nu]$$

$$\text{RMSE (linear)} = \sqrt{\frac{1}{|y|} \sum_{y_i \in y} \|y_i - y'_i\|^2} \quad (15)$$

$$\text{RMSE (log)} = \sqrt{\frac{1}{|y|} \sum_{y_i \in y} \|\log y_i - \log y'_i\|^2}$$

where y and y' are the predicted and ground truth depth images, $\delta(u, v) = \max(\frac{u}{v}, \frac{v}{u})$ and $[P]$ is the Iverson bracket which is 1 when P is true and 0 otherwise.

6.2 Experiments on SceneNet RGB-D

6.2.1 Ablation study

We first performed an ablation study on the impact of several design elements on the overall performance of the system. We use a smaller subset of SceneNet RGB-D based on 51K triplets from the first 1000 videos (selecting 50 frames from the first 1000 videos for training, and the first frame from another 1000 videos for test).

Side information We first evaluate the usage of side information from the encoder to guide the upsampling process in the decoder. We consider three variants: no side information, skip connections (Ronneberger et al., 2015) and pooling indices (Badrinarayanan et al., 2015). The results in Table 2 show that skip connections obtain worse results than no side information at all. This is caused by the fact that side information makes the decoder(s) conditioned on the *seen* encoder(s). This is problematic for *unseen* translations because the features passed through skip connections are different from those seen by the decoder during training, resulting in a drop in performance. In contrast, pooling indices provide a significant boost over no side information. Although the decoder is still conditioned to the particular seen encoders, pooling indices seem to provide helpful spatial hints to recover finer details, while being more invariant to the particular input-output combination, and even generalizing to unseen ones.

Figure 10 illustrates the differences between these three variants in depth-to-segmentation translation. Without side information the network is able to reconstruct a coarse segmentation, but without further guidance it is not able to refine it properly. Skip connections completely confuse the decoder by providing unseen encoding features. Pooling indices are able to

Side information	Pretrained	mIoU	Global
-	N	29.8%	61.6%
Skip connections	N	12.7%	50.1%
Pooling indices	N	43.2%	73.5%
Pooling indices	Y	46.7%	78.4%

Table 2: Influence of side information and RGB encoder pretraining on the final results. The task is zero-shot depth-to-semantic segmentation in SceneNet RGB-D (51K).

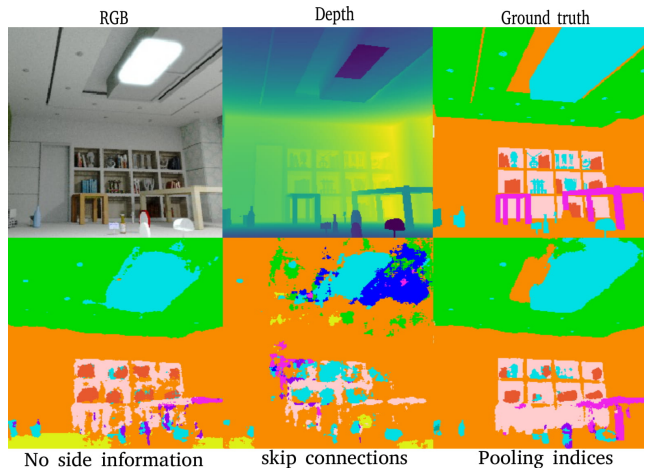


Fig. 10: Role of side information in unseen depth-to-segmentation translation in SceneNet RGB-D.

provide helpful hints about spatial structure that allows the unseen decoder to recover finer segmentation maps.

RGB pretraining We also compare training the RGB encoder from scratch and initializing with pretrained weights from ImageNet. Table 2 shows an additional gain of around 4% in mIoU when using the pretrained weights.

Given these results we perform all the remaining experiments initializing the RGB encoder with pretrained weights and use pooling indices as side information.

Latent space consistency, noise and autoencoders

We evaluate these three factors in Table 3. The results show that latent space consistency and the usage of autoencoders lead to significant performance gains; for both, the performance (in mIoU) is more than doubled. Adding noise to the output of the encoder results in a small performance gain. The results in Table 3 do not apply pooling indices for the RGB decoder (as also shown in Fig. 6). When we add pooling indices to our approach without pseudo-pairs, results drop from 46.7% to 42.4% in mIoU. This could be because we focus on unseen translations to depth or segmentation modalities, which do not include recon-

AutoEnc	Latent	Noise	PP	mIoU	Global
N	N	N	N	6.48%	15.7%
Y	N	N	N	20.3%	49.4%
Y	Y	N	N	45.8%	76.9%
Y	Y	Y	N	46.7%	78.4%
Y	Y	Y	Y	49.2%	80.5%

Table 3: Impact of several components (autoencoder, latent space consistency loss, noise and pseudo-pairs) in the performance. The task is zero-pair depth-to-segmentation in SceneNet RGB-D (51K). PP: pseudo-pairs.

structuring the RGB modality. We believe that forcing the RGB decoder to use pooling indices to reconstruct RGB images lowers the efficiency of the latent representation to reconstruct depth or segmentation. Hence, we sacrifice some of the performance translating to the RGB modality to improve the results for depth and semantic segmentation.

Pseudo-pairs We also evaluate the impact of using pseudo-pairs to exploit shared information between unseen modalities. Table 3 shows a significant gain of almost 3% in mIoU and a more moderate gain in global accuracy.

In the following sections we use the SceneNet RGB-D dataset with 170K triplets.

6.2.2 Monitoring alignment

The main challenge for M&MNet is to align the different modality-specific bottleneck features, in particular for unseen translations. We measure the alignment between the features extracted from the triplets in the test set \mathcal{D}_{DS} . For each triplet (x, y, z) (i.e. RGB, segmentation and depth images) we extract the corresponding triplet of latent features $(f_R(x), f_S(y), f_D(z))$ and measure their average pairwise cross-modal alignment. The alignment between RGB and segmentation features is measured using the following alignment factor

$$AF_{RS} = E_{(x,y) \sim \mathcal{D}_{RS}} \left[\frac{f_R(x)^\top f_S(y)}{\|f_R(x)\| \|f_S(y)\|} \right] \quad (16)$$

The other alignment factors AF_{RD} and AF_{DS} between RGB and depth features and between depth and segmentation features are defined analogously. Figure 11 shows the evolution of this alignment during training and across the different stages. The three curves follow a similar trend, with the alignment increasing in the first iterations of each stage and then stabilizing. The beginning of stage two shows a dramatic increase in the alignment, with a more moderate increase at stage three. These results are consistent with those of the ablation study of the previous section, showing that

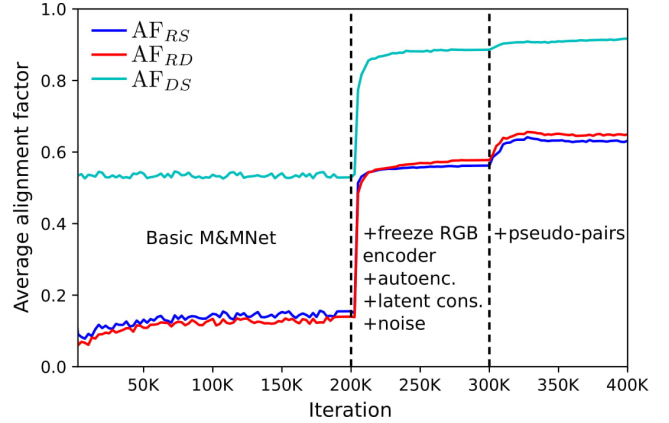


Fig. 11: Monitoring alignment between latent features on SceneNet RGB-D.

better alignment typically leads to better results in unseen translations. Overall, they show that latent space consistency, autoencoders, pseudo-pairs and pooling indices contribute to the effectiveness of M&MNet to address unseen image translation in the zero-pair setting.

6.2.3 Comparison with other models

In this section we compare M&MNet, and its variant with pseudo-pairs with several baselines:

- **CycleGAN**. We adapt CycleGAN (Zhu et al., 2017a) to learn a mapping from depth to semantic segmentation (and vice versa) in a purely unpaired setting. In contrast to M&MNet, this method only leverages depth and semantic segmentation, ignoring the available RGB data and the corresponding pairs (as shown in Figure 2a).
- **2×pix2pix**. We adapt pix2pix (Isola et al., 2017) to learn two cross-modal translations from paired data (i.e. $D \rightarrow R$ and $R \rightarrow S$). The architecture uses skip connections (which are effective in this case since both translations are seen) and the corresponding modality-specific losses. We adapt the code from (Isola et al., 2017). In contrast to ours, it requires explicit decoding to RGB, which may degrade the quality of the prediction.
- **StarGAN**. We consider two adaptations of the StarGAN (Choi et al., 2018). Both versions share the same network architecture for all modalities except for the first layer of the encoder and the last layer of decoder which are modality-specific layers. This is required since modalities vary in the number of channels. The first version, called *StarGAN(unpaired)*, uses the losses originally proposed in (Choi et al., 2018). We also implement a version which exploits the paired data, which we call *Star-*

$GAN(paired)$. For this version, we removed the cycle consistency (which is not required for paired modalities). We found this to slightly improve results.

- $D \rightarrow R \rightarrow S$ is similar to $2 \times \text{pix2pix}$ but with the architecture used in M&MNet. We train a translation model from depth to RGB and from RGB to segmentation, and obtain the transformation depth-to-segmentation by concatenating them. Note that it also requires translating to intermediate RGB images.
- $S \rightarrow R \rightarrow D$ is analogous to the previous baseline.
- **M&MNet** is the original mix and match networks (Wang et al., 2018b).
- **M&MNet+PP** is the variant of M&MNet using pseudo-pairs.
- **Oracle** is the upper bound obtained by training a translation fully supervised with paired data.

Table 4 shows results for the different methods for depth-to-segmentation translation. CycleGAN is not able to learn a good mapping, showing the difficulty of unpaired translation to solve this complex cross-modal task. $2 \times \text{pix2pix}$ manages to improve the results by resorting to the anchor modality RGB, although still not satisfactory since this sequence of translations does not enforce explicit alignment between depth and segmentation, and the first translation network may also discard information not relevant for the RGB task, but necessary for reconstructing the segmentation image (like in the Chinese whispers/telephone game). Also, both results for *StarGAN* show that this approach is unable to learn a good mapping between the unseen modalities.

M&MNet evaluated on $(D \rightarrow R \rightarrow S)$ achieve a similar result as CycleGAN, but significantly worse than $2 \times \text{pix2pix}$. However, when we run our architecture with skip connections we obtain results similar to $2 \times \text{pix2pix}$. Note that in this setting translations only involve seen encoders and decoders, so skip connections function well. The direct combination $(D \rightarrow S)$ with M&MNet outperforms all baselines significantly. The performance more than doubles in terms of mIoU. Results improve another 5% in mIoU when adding the pseudo-pairs during training.

Figure 12 shows a representative example of the differences between the evaluated methods. CycleGAN fails to recover any meaningful segmentation of the scene, revealing the difficulty to learn cross-modal translations without paired data. $2 \times \text{pix2pix}$ manages to recover the layout and coarse segmentation, but fails to segment medium and small size objects. M&MNet are able to obtain finer and more accurate segmentations.

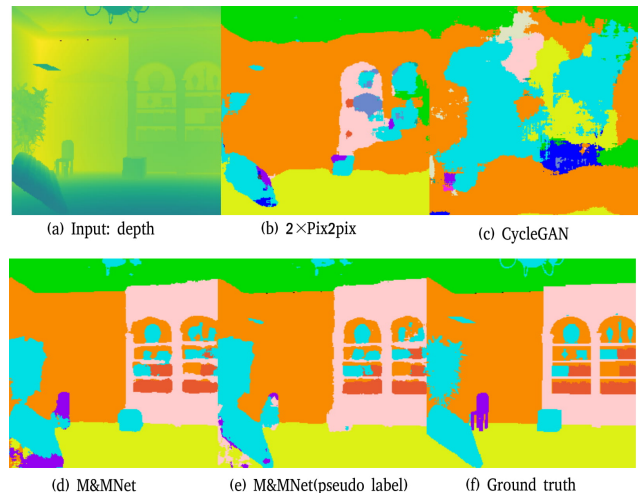


Fig. 12: Zero-pair depth-to-segmentation translation on SceneNet RGB-D.

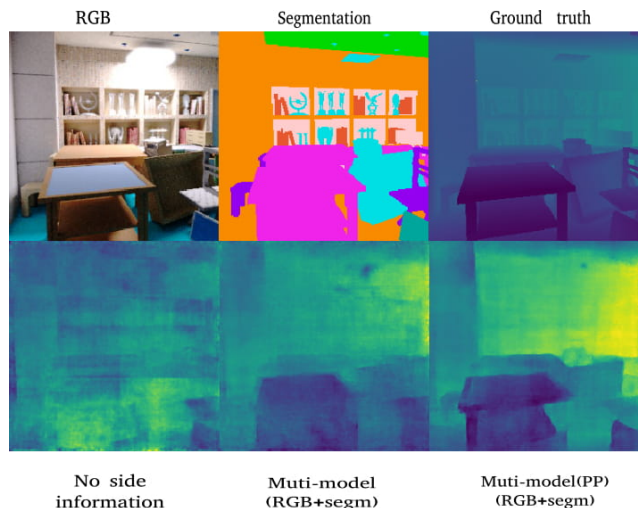


Fig. 13: Zero-pair and multimodal segmentation-to-depth on SceneNet RGB-D.

Table 5 shows results when we test in the opposite direction from semantic segmentation to depth. The conclusions are similar as in previous experiment: M&MNet outperform both baseline methods on all five evaluation metrics. Figure 13 illustrates this case, showing how pooling indices are also key to obtain good depth images, compared with no side information at all. The variant with pseudo-pairs obtains the best results.

6.2.4 Multi-modal translation

Since features from different modalities are aligned, we can also use M&MNet for multi-modal translation. For instance, in the previous multi-modal setting,

Method	Conn. L_{SEM}		Bed	Book	Ceiling	Chair	Floor	Furniture	Object	Picture	Sofa	Table	TV	Wall	Window	mIoU	Global
																	
Baselines																	
CycleGAN	SC	CE	2.79	0.00	16.9	6.81	4.48	0.92	7.43	0.57	9.48	0.92	0.31	17.4	15.1	6.34	14.2
2×pix2pix	SC	CE	34.6	1.88	70.9	20.9	63.6	17.6	14.1	0.03	38.4	10.0	4.33	67.7	20.5	25.4	57.6
StarGAN(unpaired)	PI	CE	6.71	1.42	17.6	6.21	13.2	1.25	8.51	0.52	12.8	3.24	4.28	9.52	8.57	7.21	10.7
StarGAN(paired)	PI	CE	9.70	2.56	18.4	5.70	15.7	0.41	9.20	1.56	14.2	5.02	3.56	14.7	11.4	8.62	14.1
M&MNetS $D \rightarrow R \rightarrow S$	PI	CE	0.02	0.00	8.76	0.10	2.91	2.06	1.65	0.19	0.02	0.28	0.02	58.2	3.30	5.96	32.3
M&MNetS $D \rightarrow R \rightarrow S$	SC	CE	25.4	0.26	82.7	0.44	56.6	6.30	23.6	5.42	0.54	21.9	10.0	68.6	19.6	24.7	59.7
Zero-pair																	
M&MNetS $D \rightarrow S$	PI	CE	50.8	18.9	89.8	31.6	88.7	48.3	44.9	62.1	17.8	49.9	51.9	86.2	79.2	55.4	80.4
M&MNetS+PP $D \rightarrow S$	PI	CE	52.1	29.0	88.6	32.7	86.9	66.9	48.4	76.6	25.1	45.5	58.8	88.5	82.0	60.1	82.2
Multi-modal																	
M&MNetS $(R, D) \rightarrow S$	PI	CE	49.9	25.5	88.2	31.8	86.8	56.0	45.4	70.5	17.4	46.2	57.3	87.9	79.8	57.1	81.2
M&MNetS+PP $(R, D) \rightarrow S$	PI	CE	53.3	35.7	89.9	37.0	88.6	59.3	55.8	76.9	25.7	46.6	69.6	89.5	80.0	62.2	83.5
Oracle																	
$D \rightarrow S$	PI	CE	53.7	31.0	89.1	31.4	88.2	66.8	52.7	78.4	25.7	47.4	59.3	89.7	82.2	61.2	83.4
$(R, D) \rightarrow S$	PI	CE	58.4	40.8	91.3	41.6	90.7	61.5	57.6	80.9	36.8	51.6	72.6	88.4	83.1	65.7	84.0

Table 4: Zero-pair depth-to-segmentation translation on SceneNet RGB-D. **SC**: skip connections, **PI**: pooling indexes, **CE**: cross-entropy, **PP**: pseudo-pairs. x

Method	$\delta <$			RMSE	RMSE
	1.25	1.25 ²	1.25 ³	(lin)	(log)
Baselines					
CycleGAN	0.05	0.12	0.20	4.63	1.98
2×pix2pix	0.14	0.31	0.46	3.14	1.28
StarGAN(unpaired)	0.05	0.14	0.23	4.60	1.96
StarGAN(paired)	0.07	0.15	0.26	4.58	1.94
M&MNetS $S \rightarrow R \rightarrow D$	0.15	0.30	0.44	3.24	1.24
Zero-pair					
M&MNetS $S \rightarrow D$	0.33	0.42	0.59	2.80	0.67
M&MNetS+PP $S \rightarrow D$	0.42	0.61	0.79	2.24	0.60
Multi-modal					
M&MNetS $(R, S) \rightarrow D$	0.36	0.48	0.65	2.48	0.64
M&MNetS+PP $(R, S) \rightarrow D$	0.47	0.69	0.81	1.98	0.49
Oracle					
$S \rightarrow D$	0.49	0.72	0.85	1.94	0.43
$(R, S) \rightarrow D$	0.51	0.76	0.90	1.79	0.29

Table 5: Zero-pair segmentation-to-depth on SceneNet RGB-D.

given the RGB and depth images of the same scene we can translate to segmentation. We simply combine both modality-specific latent features x and z using a weighted average $y = (1 - \alpha)x + \alpha z$, where α controls the weight of each modality. We set $\alpha = 0.2$ and use the pooling indices from the RGB encoder (instead of those from depth encoder). The resulting feature y is then decoded using the segmentation decoder. We proceed analogously to translation from RGB and segmentation to depth. The results in Table 4 and Table 5 show that this multi-modal combination further improves the performance of zero-pair translation, as the example in Figure 13 illustrates.

6.3 Experiments on SUN RGB-D

The previous results were obtained on the SceneNet RGB-D dataset which consists of synthetic images. Here we also show that M&MNetS can be effective for the more challenging dataset SUN RGB-D, which involves real images and more limited data. The results in Table 6 and Table 7 show that M&MNetS consistently outperform the other baselines in both unseen translation directions, with the new variant with pseudo-pairs obtaining the best performance. Similarly, multi-modal translation further improves the performance. Figures 15 and 16 illustrate how the proposed methods can reconstruct more reliably the target modality, especially the finer details.

The results also show that the depth cue is insufficient to detect some of the classes such as *Book* and *TV*. The oracle results show that this is also the case when you have access to depth-semantic segmentation pairs. The results also show that our multi-modal results are biased towards RGB: this is reflected in the bad results which are obtained for the class *bed* which is well detected in the depth modality but not in the RGB modality, and also not by our multi-modal system. Examples of these cases are provided in Fig. 14.

6.4 Experiments on four modalities

As an example of zero-pair translation for an application with more than three modalities we perform experiments on the Freiburg Forest dataset which contains the RGB, depth, NIR and semantic segmentation

Method	Conn. L_{SEM}		Bed	Book	Ceiling	Chair	Floor	Furniture	Object	Picture	Sofa	Table	TV	Wall	Window	mIoU	Global
			■	■	■	■	■	■	■	■	■	■	■	■	■		
Baselines																	
CycleGAN	SC	CE	0.00	0.00	0.00	17.9	46.9	1.67	4.59	0.00	0.00	18.9	0.00	29.6	25.4	11.1	26.3
2×pix2pix	SC	CE	3.88	0.00	12.4	29.6	57.1	17.2	13.0	35.4	8.07	35.1	0.00	47.0	7.73	20.5	38.6
StarGAN(unpaired)	PI	CE	0.00	0.00	2.45	15.8	33.6	5.73	6.28	0.57	0.00	6.25	0.00	28.4	26.9	9.69	20.6
StarGAN(paired)	PI	CE	0.00	0.00	2.01	20.2	38.9	4.12	5.78	0.31	0.00	7.30	0.00	31.5	30.7	10.8	23.8
M&MNet $D \rightarrow R \rightarrow S$	PI	CE	0.00	0.00	0.00	17.0	39.4	0.52	0.01	0.00	0.01	12.2	0.00	31.0	5.19	8.12	22.8
M&MNet $D \rightarrow R \rightarrow S$	SC	CE	39.9	0.25	15.2	37.6	58.0	19.0	11.7	2.45	4.82	36.9	0.00	46.8	12.3	21.9	40.6
Zero-pair																	
M&MNet $D \rightarrow S$	PI	CE	28.4	2.90	22.6	41.9	71.6	14.1	25.1	17.8	11.8	49.7	0.08	64.2	15.5	28.1	51.8
M&MNet+PP $D \rightarrow S$	PI	CE	29.8	4.52	28.5	44.1	73.3	17.2	27.5	20.1	9.81	53.4	0.14	67.5	17.9	30.2	54.2
Multi-modal																	
M&MNet $(R, D) \rightarrow S$	PI	CE	0.00	16.6	21.4	56.0	72.1	24.2	28.3	38.1	21.7	57.0	64.6	68.0	43.7	39.4	58.8
M&MNet+PP $(R, D) \rightarrow S$	PI	CE	0.10	19.3	25.5	54.6	74.6	25.6	30.1	42.4	21.0	58.1	65.2	69.0	49.7	41.1	59.8
Oracle																	
$D \rightarrow S$	PI	CE	32.6	8.01	36.5	56.8	84.7	20.4	31.4	19.7	8.75	61.7	1.60	72.1	21.2	35.1	62.3
$(R, D) \rightarrow S$	PI	CE	0.13	21.2	26.4	56.2	78.9	26.9	35.2	44.4	23.2	60.2	67.3	71.2	52.3	43.3	62.5

Table 6: Zero-pair depth-to-semantic segmentation on SUN RGB-D. **SC**: skip connections, **PI**: pooling indexes, **CE**: cross-entropy, **PP**: pseudo-pairs.

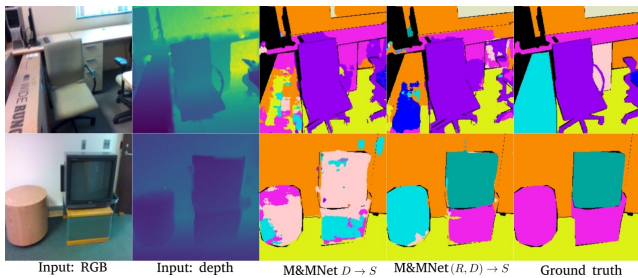


Fig. 14: Failure cases of the proposed framework on SUN RGB-D. See text for discussion.

Method	$\delta <$			RMSE	RMSE
	1.25	1.25^2	1.25^3	(lin)	(log)
Baselines					
CycleGAN	0.06	0.13	0.24	4.80	1.57
2×pix2pix	0.13	0.34	0.59	3.80	1.30
StarGAN(unpaired)	0.06	0.12	0.22	5.04	1.59
StarGAN(paired)	0.07	0.15	0.27	4.60	1.55
M&MNet $S \rightarrow R \rightarrow D$	0.12	0.35	0.62	3.90	1.36
Zero-pair					
M&MNet $S \rightarrow D$	0.45	0.66	0.78	1.75	0.53
M&MNet+PP $S \rightarrow D$	0.49	0.77	0.90	1.42	0.37
Multi-modal					
M&MNet $(R, S) \rightarrow D$	0.53	0.80	0.92	1.63	0.35
M&MNet+PP $(R, S) \rightarrow D$	0.56	0.83	0.93	1.33	0.34
Oracle					
$S \rightarrow D$	0.61	0.88	0.97	1.20	0.30
$(R, S) \rightarrow D$	0.64	0.92	0.98	0.98	0.27

Table 7: Zero-pair semantic segmentation-to-depth on SUN RGB-D.

modalities. For the training we use the settings used in the previous experiments, and add a *Berhu* loss (see Eq. 5) for NIR in this experiment.

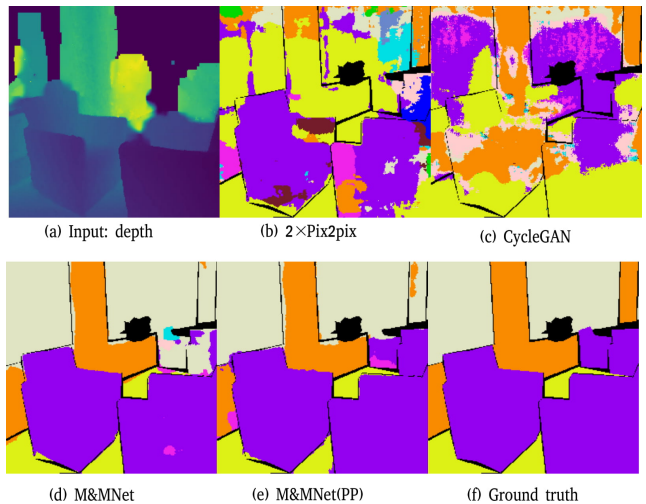


Fig. 15: Example of zero-pair depth-to-segmentation on SUN RGB-D.

In the provided dataset all modalities are recorded for all scenes, however we consider that we have pairs for RGB and semantic segmentation, and we have a non-overlapping dataset of triplets for RGB, Depth, and NIR (see Figure 17). This scenario could be considered realistic. It reflects a situation where initially the robot only has an RGB camera, and labellers have provided semantic segmentation maps for these images. Then two additional sensors are added later to the robot, but no segmentation maps are available for this newly obtained multi-modal data.

As we can see in Table 8, our method achieves the best scores. In the case of zero-pair setting (M&MNet $D \rightarrow S$, M&MNet $N \rightarrow S$, M&MNet+PP $D \rightarrow S$

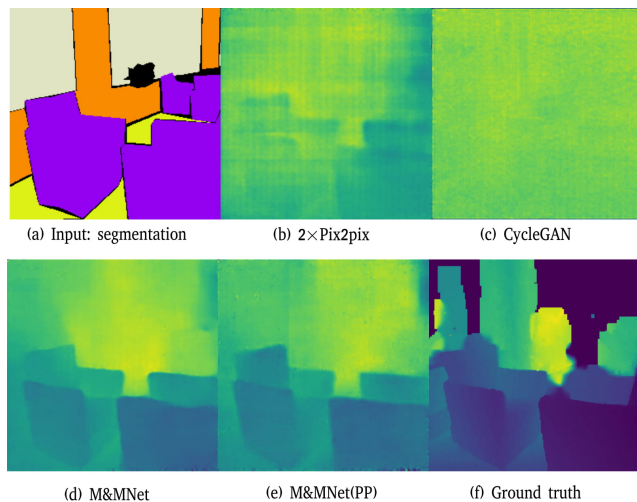


Fig. 16: Example of zero-pair segmentation-to-depth on SUN RGB-D.

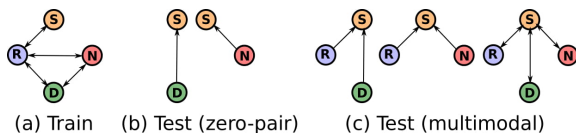


Fig. 17: Cross-modal translations in the Freiburg Forest dataset experiment: (a) training, (b) test (zero-shot) and (c) test (multimodal). We show only translations to semantic segmentation for simplicity.

and M&MNet+PP $N \rightarrow S$) the results obtain a large gap when compared to the baselines, clearly demonstrating the superiority of our method. For example, for $N \rightarrow S$ we obtain an increase of 22% over $2 \times \text{pix2pix}$. The multi-modal results show that adding more modalities further increases results. Mainly, the performance on the category *obstacle* increases. Figure 18 shows representative examples of the different methods. The conclusions are similar to previous experiments: we effectively conduct cross-modal translation with zero-pair data and pseudo-labeling further improves the results.

7 Conclusions

We have introduced mix and match networks as a framework to perform image translations between unseen modalities by leveraging the knowledge learned from seen translations with explicit training data. The key challenge lies in aligning the latent representations in the bottlenecks in such a way that any encoder-decoder combination is able to perform effectively its corresponding translation. M&MNet have advantages in terms of scalability since only seen translations need to be trained. We also introduced zero-pair

cross-modal translation, a challenging scenario involving three modalities and paired seen and unseen translations. In order to effectively address this problem, we described several tools to enforce the alignment of latent representations, including autoencoders, latent consistency losses, and robust side information. In particular, our results show that side information is critical to perform satisfactory cross-modal translations, but conventional side information such as skip connections may not work properly with unseen translations. We found that pooling indices are more robust and invariant, and provide helpful hints to guide the reconstruction of spatial structure.

We also analyzed a specific limitation of the original M&MNet (Wang et al., 2018b) in the zero-pair setting, which is that a significant part of the shared features between unseen modalities is not exploited. We proposed a variant that generates pseudo-pairs to enforce the networks to use more information between unseen modalities, even when that information is not shared by seen translations. The effectiveness of M&MNet with pseudo-pairs has been evaluated in several multi-modal datasets.

A potential limitation of our system is that we work with separate encoder and decoders for each modality. Some recent cross-domain image translators such as StarGAN (Choi et al., 2018) and SDIT (Wang et al., 2019) use a single shared encoder and a single shared decoder. In that spirit, it could be possible to have partially shared encoders and decoders between different modalities. However, modality-specific layers would be still required in more challenging cross-modal translation.

Acknowledgements The Titan Xp used for this research was donated by the NVIDIA Corporation. We acknowledge the Spanish projects TIN2016-79717-R and RTI2018-102285-A-I00, the CHISTERA project M2CR (PCIN-2015-251) and the CERCA Programme / Generalitat de Catalunya. Herranz also acknowledges the European Unions H2020 research under Marie Skłodowska-Curie grant No. 665919. Yaxing Wang acknowledges the Chinese Scholarship Council (CSC) grant No. 201507040048. .

References

- Akata Z, Perronnin F, Harchaoui Z, Schmid C (2016) Label-embedding for image classification. *IEEE Transactions on Pattern Analysis and Machine Intelligence* 38(7):1425–1438
- Alharbi Y, Smith N, Wonka P (2019) Latent filter scaling for multimodal unsupervised image-to-image translation. In: *Proceedings of the IEEE Conference*

Method	Conn.	Sky	Trail	Grass	Vegetation	Obstacle	mIoU	Global
		■	■	■	■	■		
Baselines								
CycleGAN $D \rightarrow S$	SC	36.3	31.7	19.2	24.5	5.40	23.4	26.2
CycleGAN $N \rightarrow S$	SC	37.2	34.1	18.4	29.5	0.41	23.9	28.5
$2 \times \text{pix}2\text{pix} D \rightarrow S$	SC	72.9	32.2	45.7	67.9	30.9	49.9	59.9
$2 \times \text{pix}2\text{pix} N \rightarrow S$	SC	78.6	43.2	53.4	74.4	18.6	53.6	66.8
StarGAN $D \rightarrow S$	PI	45.2	28.1	24.4	21.5	1.36	24.1	28.1
StarGAN $N \rightarrow S$	PI	31.2	15.1	29.4	23.2	10.7	21.9	25.8
M&MNet $D \rightarrow R \rightarrow S$	PI	45.3	19.6	25.4	35.5	25.3	30.0	33.5
M&MNet $N \rightarrow R \rightarrow S$	PI	58.1	34.1	32.4	42.4	12.3	35.8	42.4
Zero-pair								
M&MNet $D \rightarrow S$	PI	89.0	71.8	71.3	82.7	43.7	71.6	80.0
M&MNet $N \rightarrow S$	PI	88.1	78.1	73.4	83.1	41.0	72.7	81.0
M&MNet+PP $D \rightarrow S$	PI	89.7	75.4	72.4	83.6	45.7	73.4	81.1
M&MNet+PP $N \rightarrow S$	PI	89.9	80.1	76.9	85.5	44.2	75.3	83.5
Multi-modal								
M&MNet $(R, D) \rightarrow S$	PI	91.2	84.5	85.4	89.1	50.3	80.1	88.0
M&MNet $(R, N) \rightarrow S$	PI	91.0	83.5	85.3	90.0	52.9	80.5	88.3
M&MNet $(R, D, N) \rightarrow S$	PI	91.2	84.2	85.8	90.1	58.2	81.8	88.5
M&MNet+PP $(R, D) \rightarrow S$	PI	90.9	83.9	85.0	88.7	59.5	81.6	88.1
M&MNet+PP $(R, N) \rightarrow S$	PI	91.7	85.4	86.1	89.9	58.2	82.2	88.6
M&MNet+PP $(R, D, N) \rightarrow S$	PI	91.5	85.8	86.6	90.6	60.3	83.0	89.3
Oracle								
$D \rightarrow S$	PI	89.5	75.4	80.4	81.2	54.7	76.2	82.2
$N \rightarrow S$	PI	90.2	81.5	83.6	85.2	50.4	78.2	85.4
$(R, D, N) \rightarrow S$	PI	91.9	85.7	87.9	90.1	64.9	84.1	89.4

Table 8: Zero-pair (NIR, depth)-to-semantic segmentation on Freiburg Forest. **SC**: skip connections, **PI**: pooling indexes, **PP**: pseudo-pairs.

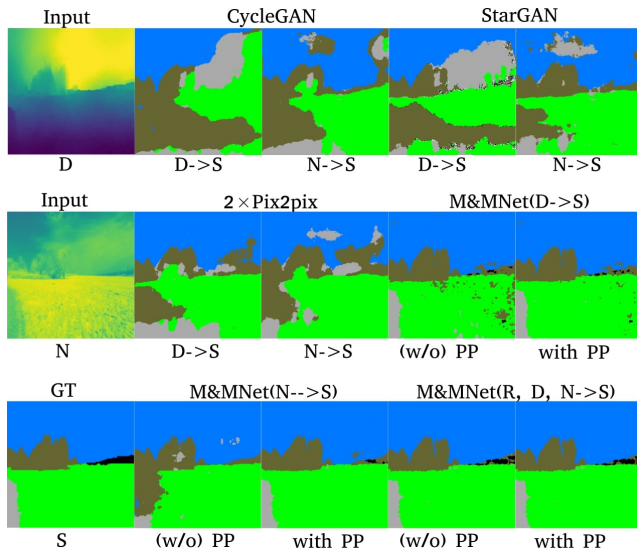


Fig. 18: Example of zero-pair translations. R: RGB, D: depth, N: NIR, S: semantic segmentation, and PP: pseudo-pairs.

on Computer Vision and Pattern Recognition, pp 1458–1466

Almahairi A, Rajeswar S, Sordani A, Bachman P, Courville A (2018) Augmented cyclegan: Learning many-to-many mappings from unpaired data. International Conference on Machine Learning

Amodio M, Krishnaswamy S (2019) Travelgan: Image-to-image translation by transformation vector learn-

ing. In: Proceedings of the IEEE Conference on Computer Vision and Pattern Recognition

Anoosheh A, Agustsson E, Timofte R, Van Gool L (2018) Combogan: Unrestrained scalability for image domain translation. 2018 IEEE/CVF Conference on Computer Vision and Pattern Recognition Workshops (CVPRW) DOI 10.1109/cvprw.2018.00122, URL <http://dx.doi.org/10.1109/CVPRW.2018.00122>

Badrinarayanan V, Handa A, Cipolla R (2015) Segnet: A deep convolutional encoder-decoder architecture for robust semantic pixel-wise labelling. Proceedings of the IEEE Conference on Computer Vision and Pattern Recognition

Cadena C, Dick AR, Reid ID (2016) Multi-modal auto-encoders as joint estimators for robotics scene understanding. In: Robotics: Science and Systems

Castrejon L, Aytar Y, Vondrick C, Pirsaviash H, Torralba A (2016) Learning aligned cross-modal representations from weakly aligned data. In: Proceedings of the IEEE Conference on Computer Vision and Pattern Recognition, pp 2940–2949

Chen LC, Papandreou G, Kokkinos I, Murphy K, Yuille AL (2018) Deeplab: Semantic image segmentation with deep convolutional nets, atrous convolution, and fully connected crfs. IEEE Transactions on Pattern Analysis and Machine Intelligence 40(4):834–848

Chen Q, Koltun V (2017) Photographic image synthesis with cascaded refinement networks. Proceedings of the International Conference on Computer Vision

Chen Y, Liu Y, Cheng Y, Li VO (2017) A teacher-student framework for zero-resource neural machine translation. arXiv preprint arXiv:170500753

Chen YC, Xu X, Tian Z, Jia J (2019) Homomorphic latent space interpolation for unpaired image-to-image translation. In: Proceedings of the IEEE Conference on Computer Vision and Pattern Recognition, pp 2408–2416

Cheng Y, Zhao X, Cai R, Li Z, Huang K, Rui Y, et al. (2016) Semi-supervised multimodal deep learning for RGB-D object recognition. Proceedings of the International Joint Conference on Artificial Intelligence

Cho W, Choi S, Park DK, Shin I, Choo J (2019) Image-to-image translation via group-wise deep whitening-and-coloring transformation. In: The IEEE Conference on Computer Vision and Pattern Recognition (CVPR)

Choi Y, Choi M, Kim M, Ha JW, Kim S, Choo J (2018) Stargan: Unified generative adversarial networks for multi-domain image-to-image translation. In: Proceedings of the IEEE Conference on Computer Vision and Pattern Recognition

- Deng J, Dong W, Socher R, Li LJ, Li K, Fei-Fei L (2009) ImageNet: A Large-Scale Hierarchical Image Database. In: Proceedings of the IEEE Conference on Computer Vision and Pattern Recognition
- Eigen D, Fergus R (2015) Predicting depth, surface normals and semantic labels with a common multi-scale convolutional architecture. In: Proceedings of the International Conference on Computer Vision, pp 2650–2658
- Eitel A, Springenberg JT, Spinello L, Riedmiller M, Burgard W (2015) Multimodal deep learning for robust rgb-d object recognition. In: Proceedings of the IEEE/RSJ Conference on Intelligent Robots and Systems, IEEE, pp 681–687
- Fergus R, Bernal H, Weiss Y, Torralba A (2010) Semantic label sharing for learning with many categories. Proceedings of the European Conference on Computer Vision pp 762–775
- Firat O, Cho K, Bengio Y (2016) Multi-way, multilingual neural machine translation with a shared attention mechanism. arXiv preprint arXiv:160101073
- Fu Y, Xiang T, Jiang YG, Xue X, Sigal L, Gong S (2017) Recent advances in zero-shot recognition. arXiv preprint arXiv:171004837
- Ganin Y, Lempitsky V (2015) Unsupervised domain adaptation by backpropagation. In: International Conference on Machine Learning, pp 1180–1189
- Gatys LA, Ecker AS, Bethge M (2016) Image style transfer using convolutional neural networks. In: Proceedings of the IEEE Conference on Computer Vision and Pattern Recognition, pp 2414–2423
- Geusebroek JM, Van den Boomgaard R, Smeulders AWM, Geerts H (2001) Color invariance. IEEE Transactions on Pattern Analysis and Machine Intelligence 23(12):1338–1350
- Gong B, Shi Y, Sha F, Grauman K (2012) Geodesic flow kernel for unsupervised domain adaptation. In: Proceedings of the IEEE Conference on Computer Vision and Pattern Recognition, IEEE, pp 2066–2073
- Gonzalez-Garcia A, van de Weijer J, Bengio Y (2018) Image-to-image translation for cross-domain disentanglement. In: Advances in Neural Information Processing Systems, pp 1294–1305
- Goodfellow I, Pouget-Abadie J, Mirza M, Xu B, Warde-Farley D, Ozair S, Courville A, Bengio Y (2014) Generative adversarial nets. In: Advances in Neural Information Processing Systems, pp 2672–2680
- Gupta S, Hoffman J, Malik J (2016) Cross modal distillation for supervision transfer. In: Proceedings of the IEEE Conference on Computer Vision and Pattern Recognition
- He K, Zhang X, Ren S, Sun J (2016) Deep residual learning for image recognition. In: Proceedings of the IEEE Conference on Computer Vision and Pattern Recognition, pp 770–778
- Hoffman J, Gupta S, Darrell T (2016a) Learning with side information through modality hallucination. In: Proceedings of the IEEE Conference on Computer Vision and Pattern Recognition, pp 826–834
- Hoffman J, Gupta S, Leong J, Guadarrama S, Darrell T (2016b) Cross-modal adaptation for rgb-d detection. In: Robotics and Automation (ICRA), 2016 IEEE International Conference on, IEEE, pp 5032–5039
- Huang X, Liu MY, Belongie S, Kautz J (2018) Multimodal unsupervised image-to-image translation. In: Proceedings of the European Conference on Computer Vision, pp 172–189
- Isola P, Zhu JY, Zhou T, Efros AA (2017) Image-to-image translation with conditional adversarial networks. Proceedings of the IEEE Conference on Computer Vision and Pattern Recognition
- Jayaraman D, Grauman K (2014) Zero-shot recognition with unreliable attributes. In: Advances in Neural Information Processing Systems, pp 3464–3472
- Johnson M, Schuster M, Le QV, Krikun M, Wu Y, Chen Z, Thorat N, Viégas F, Wattenberg M, Corrado G, et al. (2016) Google’s multilingual neural machine translation system: enabling zero-shot translation. arXiv preprint arXiv:161104558
- Kendall A, Gal Y, Cipolla R (2018) Multi-task learning using uncertainty to weigh losses for scene geometry and semantics. Proceedings of the IEEE Conference on Computer Vision and Pattern Recognition
- Kim S, Park K, Sohn K, Lin S (2016) Unified depth prediction and intrinsic image decomposition from a single image via joint convolutional neural fields. In: Proceedings of the European Conference on Computer Vision, Springer, pp 143–159
- Kim T, Cha M, Kim H, Lee J, Kim J (2017) Learning to discover cross-domain relations with generative adversarial networks. International Conference on Machine Learning
- Kingma D, Ba J (2014) Adam: A method for stochastic optimization. International Conference on Learning Representations
- Kuga R, Kanezaki A, Samejima M, Sugano Y, Matsushita Y (2017) Multi-task learning using multimodal encoder-decoder networks with shared skip connections. In: Proceedings of the International Conference on Computer Vision
- Kuznetsov Y, Stückler J, Leibe B (2017) Semi-supervised deep learning for monocular depth map prediction. In: Proceedings of the IEEE Conference on Computer Vision and Pattern Recognition, pp 6647–6655

- Lai K, Bo L, Ren X, Fox D (2011) A large-scale hierarchical multi-view rgb-d object dataset. In: Proceedings of IEEE International Conference on Robotics and Automation, IEEE, pp 1817–1824
- Laina I, Rupprecht C, Belagiannis V, Tombari F, Navab N (2016) Deeper depth prediction with fully convolutional residual networks. In: 3D Vision (3DV), 2016 Fourth International Conference on, IEEE, pp 239–248
- Lampert CH, Nickisch H, Harmeling S (2014) Attribute-based classification for zero-shot visual object categorization. *IEEE Transactions on Pattern Analysis and Machine Intelligence* 36(3):453–465
- Lee HY, Tseng HY, Huang JB, Singh M, Yang MH (2018) Diverse image-to-image translation via disentangled representations. In: Proceedings of the European Conference on Computer Vision, pp 35–51
- Li Y, Liu MY, Li X, Yang MH, Kautz J (2018) A closed-form solution to photorealistic image stylization. In: Proceedings of the European Conference on Computer Vision, pp 453–468
- Lin J, Xia Y, Qin T, Chen Z, Liu TY (2018) Conditional image-to-image translation. In: Proceedings of the IEEE Conference on Computer Vision and Pattern Recognition, pp 5524–5532
- Liu F, Shen C, Lin G, Reid I (2016) Learning depth from single monocular images using deep convolutional neural fields. *IEEE Transactions on Pattern Analysis and Machine Intelligence* 38(10):2024–2039
- Liu MY, Breuel T, Kautz J (2017) Unsupervised image-to-image translation networks. *Advances in Neural Information Processing Systems*
- Long J, Shelhamer E, Darrell T (2015) Fully convolutional networks for semantic segmentation. In: Proceedings of the IEEE Conference on Computer Vision and Pattern Recognition, pp 3431–3440
- Mao X, Li Q, Xie H, Lau RY, Wang Z (2016) Multi-class generative adversarial networks with the l2 loss function. arXiv preprint arXiv:161104076
- Mathieu MF, Zhao JJ, Zhao J, Ramesh A, Sprechmann P, LeCun Y (2016) Disentangling factors of variation in deep representation using adversarial training. In: *Advances in Neural Information Processing Systems*, pp 5040–5048
- McCormac J, Handa A, Leutenegger S, JDavison A (2017) Scenenet rgb-d: Can 5m synthetic images beat generic imagenet pre-training on indoor segmentation? Proceedings of the International Conference on Computer Vision
- Mejjati YA, Richardt C, Tompkin J, Cosker D, Kim KI (2018) Unsupervised attention-guided image-to-image translation. In: *Advances in Neural Information Processing Systems*, pp 3697–3707
- Mirza M, Osindero S (2014) Conditional generative adversarial nets. arXiv preprint arXiv:14111784
- Ngiam J, Khosla A, Kim M, Nam J, Lee H, Ng AY (2011) Multimodal deep learning. In: *International Conference on Machine Learning*, pp 689–696
- Nilsback ME, Zisserman A (2008) Automated flower classification over a large number of classes. In: *Computer Vision, Graphics & Image Processing, 2008. ICVGIP'08. Sixth Indian Conference on*, IEEE, pp 722–729
- Perarnau G, Van De Weijer J, Raducanu B, Álvarez JM (2016) Invertible conditional gans for image editing. arXiv preprint arXiv:161106355
- Reed S, Akata Z, Lee H, Schiele B (2016) Learning deep representations of fine-grained visual descriptions. In: *Proceedings of the IEEE Conference on Computer Vision and Pattern Recognition*, pp 49–58
- Rohrbach M, Stark M, Schiele B (2011) Evaluating knowledge transfer and zero-shot learning in a large-scale setting. In: *Proceedings of the IEEE Conference on Computer Vision and Pattern Recognition*, IEEE, pp 1641–1648
- Ronneberger O, Fischer P, Brox T (2015) U-net: Convolutional networks for biomedical image segmentation. In: *International Conference on Medical image computing and computer-assisted intervention*, Springer, pp 234–241
- Roy A, Todorovic S (2016) Monocular depth estimation using neural regression forest. In: *Proceedings of the IEEE Conference on Computer Vision and Pattern Recognition*, pp 5506–5514
- Saito K, Ushiku Y, Harada T (2017) Asymmetric tri-training for unsupervised domain adaptation. *International Conference on Machine Learning*
- Silberman N, Hoiem D, Kohli P, Fergus R (2012) Indoor segmentation and support inference from RGB-D images. In: *Proceedings of the European Conference on Computer Vision*, Springer, pp 746–760
- Simonyan K, Zisserman A (2015) Very deep convolutional networks for large-scale image recognition. *International Conference on Learning Representations*
- Song S, Lichtenberg SP, Xiao J (2015) Sun rgb-d: A rgb-d scene understanding benchmark suite. In: *Proceedings of the IEEE Conference on Computer Vision and Pattern Recognition*, pp 567–576
- Song X, Herranz L, Jiang S (2017) Depth CNNs for RGB-D scene recognition: learning from scratch better than transferring from rgb-cnns. In: *Proceedings of the AAAI Conference on Artificial Intelligence*
- Taigman Y, Polyak A, Wolf L (2017) Unsupervised cross-domain image generation. *International Conference on Learning Representations*

- Tsai YH, Hung WC, Schulter S, Sohn K, Yang MH, Chandraker M (2018) Learning to adapt structured output space for semantic segmentation. *Proceedings of the IEEE Conference on Computer Vision and Pattern Recognition*
- Valada A, Oliveira GL, Brox T, Burgard W (2016) Deep multispectral semantic scene understanding of forested environments using multimodal fusion. In: *International Symposium on Experimental Robotics*, Springer, pp 465–477
- Wang P, Shen X, Lin Z, Cohen S, Price B, Yuille AL (2015) Towards unified depth and semantic prediction from a single image. In: *Proceedings of the IEEE Conference on Computer Vision and Pattern Recognition*, pp 2800–2809
- Wang TC, Liu MY, Zhu JY, Tao A, Kautz J, Catanzaro B (2018a) High-resolution image synthesis and semantic manipulation with conditional gans. In: *Proceedings of the IEEE Conference on Computer Vision and Pattern Recognition*, pp 8798–8807
- Wang W, Neumann U (2018) Depth-aware CNN for RGB-D segmentation. In: *Proceedings of the European Conference on Computer Vision*, pp 135–150
- Wang Y, van de Weijer J, Herranz L (2018b) Mix and match networks: encoder-decoder alignment for zero-pair image translation. In: *Proceedings of the IEEE Conference on Computer Vision and Pattern Recognition*, pp 5467–5476
- Wang Y, Gonzalez-Garcia A, van de Weijer J, Herranz L (2019) Sdit: Scalable and diverse cross-domain image translation. *arXiv preprint arXiv:190806881*
- Wu W, Cao K, Li C, Qian C, Loy CC (2019) Transgaga: Geometry-aware unsupervised image-to-image translation. In: *The IEEE Conference on Computer Vision and Pattern Recognition (CVPR)*
- Wu Z, Han X, Lin YL, Uzunbas MG, Goldstein T, Lim SN, Davis LS (2018) Dcan: Dual channel-wise alignment networks for unsupervised scene adaptation. In: *Proceedings of the European Conference on Computer Vision*
- Xian Y, Lampert CH, Schiele B, Akata Z (2018a) Zero-shot learning—a comprehensive evaluation of the good, the bad and the ugly. *IEEE Transactions on Pattern Analysis and Machine Intelligence*
- Xian Y, Lorenz T, Schiele B, Akata Z (2018b) Feature generating networks for zero-shot learning. In: *Proceedings of the IEEE Conference on Computer Vision and Pattern Recognition*, pp 5542–5551
- Xu D, Ouyang W, Ricci E, Wang X, Sebe N (2017) Learning cross-modal deep representations for robust pedestrian detection. In: *Proceedings of the IEEE Conference on Computer Vision and Pattern Recognition*, pp 5363–5371
- Yi Z, Zhang H, Gong PT, et al. (2017) Dualgan: Unsupervised dual learning for image-to-image translation. In: *Proceedings of the International Conference on Computer Vision*
- Yu F, Koltun V (2016) Multi-scale context aggregation by dilated convolutions. *International Conference on Learning Representations*
- Yu L, Zhang L, van de Weijer J, Khan FS, Cheng Y, Parraga CA (2018) Beyond eleven color names for image understanding. *Machine Vision and Applications* 29(2):361–373
- Zhang L, Gonzalez-Garcia A, van de Weijer J, Danelljan M, Khan FS (2019) Synthetic data generation for end-to-end thermal infrared tracking. *IEEE Transactions on Image Processing* 28(4):1837–1850
- Zhang R, Isola P, Efros AA (2016) Colorful image colorization. In: *Proceedings of the European Conference on Computer Vision*, Springer, pp 649–666
- Zhao H, Shi J, Qi X, Wang X, Jia J (2017) Pyramid scene parsing network. In: *Proceedings of the IEEE Conference on Computer Vision and Pattern Recognition*, pp 2881–2890
- Zheng H, Cheng Y, Liu Y (2017) Maximum expected likelihood estimation for zero-resource neural machine translation. In: *Proceedings of the International Joint Conference on Artificial Intelligence*
- Zhu JY, Park T, Isola P, Efros AA (2017a) Unpaired image-to-image translation using cycle-consistent adversarial networks. In: *Proceedings of the International Conference on Computer Vision*
- Zhu JY, Zhang R, Pathak D, Darrell T, Efros AA, Wang O, Shechtman E (2017b) Toward multimodal image-to-image translation. In: *Advances in Neural Information Processing Systems*, pp 465–476
- Zou Y, Yu Z, Vijaya Kumar B, Wang J (2018) Unsupervised domain adaptation for semantic segmentation via class-balanced self-training. In: *Proceedings of the European Conference on Computer Vision*

A Appendix: Network architecture on RGB-D or RGB-D-NIR dataset

Table 9 shows the architecture (convolutional and pooling layers) of the encoders used in the cross-modal experiment. Tables 10 and 11 show the corresponding decoders. Table 12 shows the discriminator used for RGB. Every convolutional layer of the encoders, decoders and the discriminator is followed by a batch normalization layer and a ReLU layer (LeakyReLU for the discriminator). The only exception is the RGB encoder, which is initialized with weights from the VGG16 model pretrained on imageNet (Simonyan and Zisserman, 2015) and does not use batch normalization. The used abbreviations are shown in Table 16.

Layer	Input → Output	Kernel, stride
conv1 (RGB)	[6,256,256,3] → [6,256,256,64]	[3,3], 1
conv1 (Depth)	[6, 256, 256, 1] → [6, 256, 256, 64]	[3,3], 1
conv1 (NIR)	[6, 256, 256, 1] → [6, 256, 256, 64]	[3,3], 1
conv1 (Segm.)	[6,256,256,14] → [6,256,256,64]	[3,3], 1
conv2	[6,256,256,64] → [6,256,256,64]	[3,3], 1
pool2 (max)	[6,256,256,64] → [6,128,128,64]+indices2	[2,2], 2
conv3	[6,128,128,64] → [6,128,128,128]	[3,3], 1
conv4	[6,128,128,128] → [6,128,128,128]	[3,3], 1
pool4 (max)	[6,128,128,128] → [6,64,64,128]+indices4	[2,2], 2
conv5	[6,64,64,128] → [6,64,64,256]	[3,3], 1
conv6	[6,64,64,256] → [6,64,64,256]	[3,3], 1
conv7	[6,64,64,256] → [6,64,64,256]	[3,3], 1
pool7 (max)	[6,64,64,256] → [6,32,32,256]+indices7	[2,2], 2
conv8	[6,32,32,256] → [6,32,32,512]	[3,3], 1
conv9	[6,32,32,512] → [6,32,32,512]	[3,3], 1
conv10	[6,32,32,512] → [6,32,32,512]	[3,3], 1
pool10 (max)	[6,32,32,512] → [6,16,16,512]+indices10	[2,2], 2
conv11	[6,16,16,512] → [6,16,16,512]	[3,3], 1
conv12	[6,16,16,512] → [6,16,16,512]	[3,3], 1
conv13	[6,16,16,512] → [6,16,16,512]	[3,3], 1
relu13	[6,16,16,512] → [6,16,16,512]	-, -
pool13 (max)	[6,16,16,512] → [6,8,8,512]+indices13	[2,2], 2

Table 9: The architecture of the encoder of RGB, depth, NIR and semantic segmentation.

B Appendix: Network architecture on the color dataset and the artworks dataset

We use several datasets to verify the generality of our method, including object (Color) and scenes (Artworks).

Color dataset (Yu et al., 2018). We consider the object dataset for color which is collected by Yu et al. (2018), which includes 11 color labels, each category containing 1000 images. We resize all images to 128×128 .

Artworks (Zhu et al., 2017a). We also illustrate M&MNet in an artwork setting. This includes real images (*photo*) and four artistic styles (*Monet, van Gogh, Ukiyo-e* and *Cezanne*). The set contains 3000 (*photo*), 800 (*Ukiyo-e*), 500 (*van Gogh*), 600 (*Cezanne*) and 1200 (*Monet*) images. All images are resized to 256×256 .

We consider Adam (Kingma and Ba, 2014) with a batch size of 4, using a learning rate of 0.0002. The network is initialized using a Gaussian distribution with zero mean and a standard deviation of 0.5. We only use adversarial loss to train our model.

Tables 13-15 show the architectures of the encoder, image decoder and discriminator used in the cross-modal experiment. The following tables only show the image size of 128×128 , while for artworks dataset it is same architecture except for image resolution. The used abbreviations are shown in Table 16.

C Appendix: Network architecture for the Flower dataset

Flower dataset (Nilsback and Zisserman, 2008). The Flower dataset consists of 102 categories. We consider 10 categories (*passionflower, petunia, rose, wallflower, watercress, waterlily, cyclamen, foxglove, frangipani, hibiscus*). Each category includes between 100 and 258 images. we resize the image to 128×128 .

Similarly, we optimize our model by means of using Adam (Kingma and Ba, 2014), the batch size of 4 and a learning rate of 0.0002. We initialize hyperparameters using

layer	Input → Output	Kernel, stride
unpool1	indices13 + [6,8,8,512] → [6, 16, 16, 512]	[2, 2], 2
conv1	[6,16,16,512] → [6, 16, 16, 512]	[3,3], 1
BN1	[6,16,16,512] → [6, 16, 16, 512]	-, -
relu1	[6,16,16,512] → [6, 16, 16, 512]	-, -
conv2	[6,16,16,512] → [6, 16, 16, 512]	[3,3], 1
BN2	[6,16,16,512] → [6, 16, 16, 512]	-, -
relu2	[6,16,16,512] → [6, 16, 16, 512]	-, -
conv3	[6,16,16,512] → [6, 16, 16, 512]	[3,3], 1
BN3	[6,16,16,512] → [6, 16, 16, 512]	-, -
relu3	[6,16,16,512] → [6, 16, 16, 512]	-, -
unpool4	indices10 + [6,16,16,512] → [6, 32, 32, 512]	[2, 2], 2
conv4	[6,32,32,512] → [6, 32, 32, 512]	[3,3], 1
BN4	[6,32,32,512] → [6, 32, 32, 512]	-, -
relu4	[6,32,32,512] → [6, 32, 32, 512]	-, -
conv5	[6,32,32,512] → [6, 32, 32, 512]	[3,3], 1
BN5	[6,32,32,512] → [6, 32, 32, 512]	-, -
relu5	[6,32,32,512] → [6, 32, 32, 512]	-, -
conv6	[6,32,32,512] → [6, 32, 32, 256]	[3,3], 1
BN6	[6,32,32,512] → [6, 32, 32, 512]	-, -
relu6	[6,32,32,512] → [6, 32, 32, 512]	-, -
unpool7	indices7 + [6,32,32,256] → [6, 64, 64, 256]	[2, 2], 2
conv7	[6,64,64,256] → [6, 64, 64, 256]	[3,3], 1
BN7	[6,64,64,256] → [6, 64, 64, 256]	-, -
relu7	[6,64,64,256] → [6, 64, 64, 256]	-, -
conv8	[6,64,64,256] → [6, 64, 64, 256]	[3,3], 1
BN8	[6,64,64,256] → [6, 64, 64, 256]	-, -
relu8	[6,64,64,256] → [6, 64, 64, 256]	-, -
conv9	[6,64,64,256] → [6, 64, 64, 128]	[3,3], 1
BN9	[6,64,64,256] → [6, 64, 64, 256]	-, -
relu9	[6,64,64,256] → [6, 64, 64, 256]	-, -
unpool10	indices4 + [6,64,64,128] → [6, 128, 128, 128]	[2, 2], 2
conv10	[6,128,128,128] → [6, 128, 128, 128]	[3,3], 1
BN10	[6,128,128,128] → [6, 128, 128, 128]	-, -
relu10	[6,128,128,128] → [6, 128, 128, 128]	-, -
conv11	[6,128,128,128] → [6, 128, 128, 64]	[3,3], 1
BN11	[6,128,128,128] → [6, 128, 128, 128]	-, -
relu11	[6,128,128,128] → [6, 128, 128, 128]	-, -
unpool12	indices2 + [6,128,128,64] → [6, 256, 256, 64]	[2, 2], 2
conv12	[6,256,256,64] → [6, 256, 256, 64]	[3,3], 1
conv13 (Depth)	[6,256,256,64] → [6, 256, 256, 1]	[3,3], 1
conv13 (NIR)	[6,256,256,64] → [6, 256, 256, 5]	[3,3], 1
conv13 (Segm.)	[6,256,256,64] → [6, 256, 256, 14]	[3,3], 1

Table 10: The architecture of the decoder of depth, NIR and semantic segmentation.

layer	Input → Output	Kernel, stride
conv1	[6,8,8,512] → [6, 16, 16, 512]	[3, 3], 1
BN1	[6,16,16,512] → [6, 16, 16, 512]	-, -
relu1	[6,16,16,512] → [6, 16, 16, 512]	-, -
conv2	[6,16,16,512] → [6, 32, 32, 256]	[3, 3], 1
BN2	[6,32,32,256] → [6, 32, 32, 256]	-, -
relu2	[6,32,32,256] → [6, 32, 32, 256]	-, -
conv3	[6,32,32,256] → [6, 64, 64, 128]	[3, 3], 1
BN3	[6,64,64,128] → [6, 64, 64, 128]	-, -
relu3	[6,64,64,128] → [6, 64, 64, 128]	-, -
conv4	[6,64,64,128] → [6, 128, 128, 64]	[3, 3], 1
BN4	[6,128,128,64] → [6, 128, 128, 64]	-, -
relu4	[6,128,128,64] → [6, 128, 128, 64]	-, -
conv5	[6,128,128,64] → [6, 256, 256, 3]	[3, 3], 1

Table 11: The architecture of the decoder of RGB

a Gaussian distribution with zero mean and a standard deviation of 0.5. We use adversarial loss and $L2$ to train Θ_3 , and only $L2$ for Θ_1 and Θ_2 .

Tables 17 and 18 detail the architecture of the encoder and decoder, respectively, of the two single channel modalities Θ_1 and Θ_2 . The encoder and decoder for the third modality Θ_3 are analogous, just adapted to three input and output channels, respectively. For Θ_3 we also use the discriminator detailed in Table 15.

layer	Input →Output	Kernel, stride
deconv1	[6, 256, 256, 3] → [6, 128, 128, 64]	[5, 5], 2
lrelu1	[6, 128, 128, 64] → [6, 128, 128, 64]	-, -
deconv2	[6, 128, 128, 64] → [6, 64, 64, 128]	[5, 5], 2
lrelu2	[6, 64, 64, 128] → [6, 64, 64, 128]	-, -
deconv3	[6, 64, 64, 128] → [6, 32, 32, 256]	[5,5], 2
lrelu3	[6, 32, 32, 256] → [6, 32, 32, 256]	-, -
deconv4	[6, 32, 32, 256] → [6, 16, 16, 512]	[5,5], 2

Table 12: RGB discriminator.

Layer	Input →Output	Kernel, stride, pad
conv1	[4,128, 128,3] → [4,128, 128, 64]	[7,7], 1, 3
IN1	[4,128, 128, 64] → [4,128, 128, 64]	-, -, -
pool1 (max)	[4,128, 128, 64] → [4,64, 64, 64]+indices1	[2,2], 2, -
conv2	[4,64, 64,64] → [4,64, 64,128]	[7,7], 1, 3
IN2	[4,64, 64,128] → [4,64, 64,128]	-, -, -
pool2 (max)	[4,64, 64,128] → [4,32, 32,128]+indices2	[2,2], 2, -
conv3	[4,32, 32,128] → [4,32, 32,256]	[7,7], 1, 3
IN3	[4,32, 32,256] → [4,32, 32,256]	-, -, -
pool3 (max)	[4,32, 32,256] → [4,16, 16,256]+indices3	[2,2], 2, -
RB(IN)4-9	[4,16, 16,256] → [4,16, 16,256]	[7,7], 1, 3

Table 13: The architecture of the encoder for 128×128 input.

Layer	Input →Output	Kernel, stride, pad
RB(IN)1-6	[4,16, 16,256] → [4,16, 16,256]	[7,7], 1, 3
unpool1	indices3 + [4,16, 16,256] → [4,32, 32,256]	[2, 2], 2, -
conv1	[4,32, 32,256] → [4,32, 32,128]	[7,7], 1, 3
IN1	[4,32, 32,128] → [4,32, 32,128]	-, -, -
unpool2	indices2 + [4,32, 32,128] → [4, 64, 64,128]	[2, 2], 2, -
conv2	[4, 64, 64,128] → [4, 64, 64,64]	[7,7], 1, 3
IN2	[4, 64, 64,64] → [4, 64, 64,64]	-, -, -
unpool3	indices1 + [4, 64, 64,64] → [4, 128, 128,64]	[2, 2], 2, -
conv3	[4, 128, 128,64] → [4, 128, 128,3]	[7,7], 1, 3

Table 14: The architecture of the decoder for 128×128 output.

Layer	Input →Output	Kernel, stride, pad
conv1	[4,128, 128,3] → [4,64, 64,64]	[4,4], 2, 1
lrelu1	[4,64, 64,64] → [4,64, 64,64]	-, -, -
conv2	[4,64, 64,64] → [4,32, 32,128]	[4,4], 2, 1
lrelu2	[4,32, 32,128] → [4,32, 32,128]	-, -, -
conv3	[4,32, 32,128] → [4,16, 16,256]	[4,4], 2, 1
lrelu3	[4,16, 16,256] → [4,16, 16,256]	-, -, -
conv4	[4,16, 16,256] → [4,8, 8,512]	[4,4], 2, 1
lrelu4	[4,8, 8,512] → [4,8, 8,512]	-, -, -
conv5	[4,8, 8,512] → [4,8, 8,1]	[1,1], 1, 0

Table 15: Architecture for the discriminator Loss specification for 128×128 input.

Abbreviation	Name
pool	pooling layer
unpool	unpooling layer
lrelu	leaky relu layer
conv	convolutional layer
linear	fully connection layer
BN	batch normalization layer
IN	instance normalization layer
RB(IN)	residual block layer using instance normalization

Table 16: Abbreviations used in other tables.

Layer	Input →Output	Kernel, stride, pad
conv1	[4,128, 128,1] → [4,128, 128, 64]	[7,7], 1, 3
IN1	[4,128, 128, 64] → [4,128, 128, 64]	-, -, -
pool1 (max)	[4,128, 128, 64] → [4,64, 64, 64]+indices1	[2,2], 2, -
conv2	[4,64, 64,64] → [4,64, 64,128]	[7,7], 1, 3
IN2	[4,64, 64,128] → [4,64, 64,128]	-, -, -
pool2 (max)	[4,64, 64,128] → [4,32, 32,128]+indices2	[2,2], 2, -
conv3	[4,32, 32,128] → [4,32, 32,256]	[7,7], 1, 3
IN3	[4,32, 32,256] → [4,32, 32,256]	-, -, -
pool3 (max)	[4,32, 32,256] → [4,16, 16,256]+indices3	[2,2], 2, -
RB(IN)4-9	[4,16, 16,256] → [4,16, 16,256]	[7,7], 1, 3

Table 17: The architecture of the encoder of Θ_1 and Θ_2 .

Layer	Input →Output	Kernel, stride, pad
RB(IN)1-6	[4,16, 16,256] → [4,16, 16,256]	[7,7], 1, 3
unpool1	indices3 + [4,16, 16,256] → [4,32, 32,256]	[2, 2], 2, -
conv1	[4,32, 32,256] → [4,32, 32,128]	[7,7], 1, 3
IN1	[4,32, 32,128] → [4,32, 32,128]	-, -, -
unpool2	indices2 + [4,32, 32,128] → [4, 64, 64,128]	[2, 2], 2, -
conv2	[4, 64, 64,128] → [4, 64, 64,64]	[7,7], 1, 3
IN2	[4, 64, 64,64] → [4, 64, 64,64]	-, -, -
unpool3	indices1 + [4, 64, 64,64] → [4, 128, 128,64]	[2, 2], 2, -
conv3	[4, 128, 128,64] → [4, 128, 128,1]	[7,7], 1, 3

Table 18: The architecture of the decoder for Θ_1 and Θ_2 .